



HAL
open science

Blast waves propagation and their mitigation

Steven Kerampran, M. Arrigoni, Paul Locking

► **To cite this version:**

Steven Kerampran, M. Arrigoni, Paul Locking. Blast waves propagation and their mitigation. Greener and safer energetic and ballistic systems, Military Technical Academy Publishing House, pp.205-252, 2016, 978-973-640-252-4. hal-01714103

HAL Id: hal-01714103

<https://ensta-bretagne.hal.science/hal-01714103>

Submitted on 21 Feb 2018

HAL is a multi-disciplinary open access archive for the deposit and dissemination of scientific research documents, whether they are published or not. The documents may come from teaching and research institutions in France or abroad, or from public or private research centers.

L'archive ouverte pluridisciplinaire **HAL**, est destinée au dépôt et à la diffusion de documents scientifiques de niveau recherche, publiés ou non, émanant des établissements d'enseignement et de recherche français ou étrangers, des laboratoires publics ou privés.

Blast waves propagation and their mitigation

M. Arrigoni, S. Kerampran
ENSTA Bretagne, 2 rue François Verny, 29806 Brest cedex 09, France

P. Locking, BAE, UK

1. Introduction

This course is given in the frame of an ERASMSUS+ program untitled “Greener and Safer Energetic and Ballistic Systems” (GSEBS). It has been written with the purpose of knowledge dissemination, dealing with blast wave generation, Blast propagation in a fluid and compressible media. The goal of this lecture is also to give engineers and researchers a sufficient knowledge for approaching blast wave problems by deducing the blast loading, which is the input data of the fluid-structure interaction that can be solved by using computational methods. It is particularly needed in design of critical infrastructures because they are the target of terrorist threats, which are nowadays a major worry of European nations. A focus will be done on blast mitigation. A part of the presented knowledge gathered in this course is taken from the Unified Facility Criteria n°3-340-2 “Structures to resist the effects of accidental explosions” [UFC-3-340-2, 2014], which is a reference in knowhow for designing critical infrastructures. A large contribution has been taken from scientific papers. Some exercises are given in order to guide the reader.

The lecture is organised as follow. Paragraph 2 gives some generalities about energetic materials that are at the origin of blast waves. Paragraph 3 describes the blast wave and its evolution. The following paragraph introduces the similitude laws that make able to study blast wave in reduced scale and gives the evolution of main blast characteristic versus the reduced distance. Paragraph 5 discusses the notion of TNT equivalent. In the sixth paragraph are given some principles of experimental measurement of blast waves. In the seventh paragraph planar oblique shock waves are presented. In the last paragraph, some blast mitigation techniques are presented.

2. Energetic materials

Energetic materials are deeper detailed in the previous chapters. Only generalities are given in this paragraph.

Three families

Energetic materials have, within their molecules, their own combustive and oxidizer, that are in an intimate contact, allowing thus a fast chemical decomposition. They fall into three main categories that are powders, propellants and high explosives (fig. 2.1). Powders are mainly used for ballistic ammunitions and in some pyromechanisms. Propellants are used in rockets propulsion and airbag systems. High explosives are not only used in weaponry but also in mining and process industries. The energy provided by their use is about 5 MJ/kg, which is much lower than the one given by the combustion of 1 kg of fuel (20 MJ), but it is delivered within a very short time, what explains the most important power and thermo-mechanical effects. They find major applications in

defence and industrial fields. Producing safer and greener energetic materials is still a challenge nowadays. Energetic materials are the objects of international regulations and classifications for transportation [UN, 2009].

The black powder is known as the historically first energetic material produced by humans. A recipe of this last was given in 1044 AD in the "Wujing Zongyao" or "Collection of the Most Important Military Techniques". This recipe migrated along the Silk Road and has been successfully introduced in European battlefield (Crécy, 1346). Black powder also found civilian uses: the power of the black powder allowed digging the "Canal du Midi" in the south of France from 1666 to 1681, which is nowadays designated as a UNESCO world Heritage site.

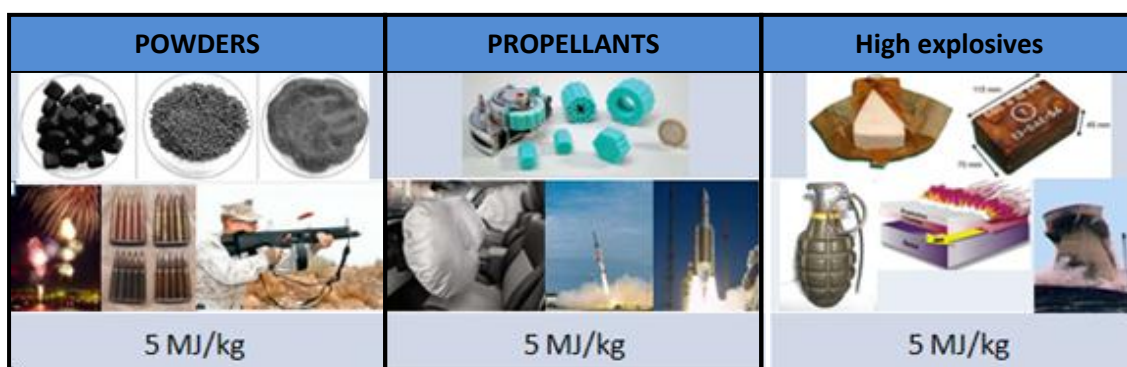


Figure 2.1 : Energetic materials are classified into three categories, powders, propellants and high explosives.

Mixture of $C_xH_yO_zN_w$ explosives

Meyer proposed a method for calculating the detonation energy of explosive mixtures [Meyer, 2007]. In its example, he considered an explosive mixture of organic components presented in table 1.

The first step consists in calculating the energy of formation of the mixture from Energies of formation of each components weighted by their mass ratio. It gives an equivalent energy of formation $E_{f\ composition} = -767.91\ kcal/kg$

Component	Formula	% mass.	E_f kcal/kg	% E_f kcal/kg
Nitro-glycerine	$C_3H_5O_9N_3$	8	-368	-29.44
Nitroglycol	$C_2H_4O_6N_2$	30	-358.2	-107.46
Nitrocellulose 12.5% N	$C_{12}H_{14}O_{22}N_6$	1.5	-605.6	-9.08
Ammonium Nitrate	$H_4O_3N_2$	53.5	-1058	-566.03
Dinitrotoluene	$C_7H_8O_4N_2$	2	-70	-1.40
Wood dust	-	5	-1090	-54.5

Table 1: Explosive mixture composition [Meyer, 2007].

- Second step consists in considering the content of each monoconstituant C, H, O, N in 1 kg of composition. It can be done for each organic component by determining a factor K (2.1):

$$K = \frac{1000g}{M_{\text{explosif}} (g/mol)} \quad (2.1)$$

The coefficients x, y, z, w of the molar composition for each organic components are multiplied by the factor K , what gives $C_{xK}H_{yK}O_{zK}N_{wK}$. By weighting by the mass ratio, the respective contribution of C, H, O, N of each organic component to the total mixture can be determined (table 2). The equivalent shortened formula of the mixture can be given for 1 kg of this mixture: $C_{8.19}H_{40.48}O_{37.39}N_{18.73}$.

Component	C	H	O	N
Nitroglycerine - 8%	1.057	1.762	3.170	1.057
Nitroglycol - 30 %	3.945	7.890	11.835	3.945
Nitrocellulose 12.5% N – 1.5 %	0.332	0.420	0.545	0.134
Ammonium Nitrate – 53.5 %	-	26.73	20.052	13.370
Dinitrotoluène – 2 %	0.769	0.659	0.439	0.220
Wood dust -	2.085	3.03	1.35	-
<i>Total</i>	<i>8.19</i>	<i>40.48</i>	<i>37.39</i>	<i>18.73</i>

Table 2 : Detailed explosive composition [Meyer, 2007].

- *Exercise 1: Apply the Meyer method to the "Composition B" explosive mixture, made of 64% of RDX ($C_3H_6O_6N_6$) and 36% of TNT ($C_7H_5O_6N_3$).*

Oxygen balance of $C_xH_yO_zN_w$ energetic materials

The maximum specific energy emitted by an energetic material will be obtained for a complete oxidation of the reactive mixture, it means not default of oxygen, neither excess of it. Actually, it is not the case for the major part of high explosives. The oxygen balance has to be then considered. In $C_xH_yO_zN_w$ explosives, the oxygen balance OB is defined by formula (2.2) and can be either negative (under oxygenate) or positive (over oxygenate):

$$BO = \frac{M_o}{M_{\text{explosif}}} \left(z - 2x - \frac{y}{2} \right) \quad (2.2)$$

Example: The oxygen balance of 1 kg of the mixture presented in table 2 is 12%. The explosive mixture is over oxygenated.

- *Exercise 2: Calculate the oxygen balance of the Composition B.*

Various regimes of decomposition

Berthelot and Vieille (1881) [Krehl, 2008] showed that three regimes of chemical decomposition could exist: Combustion, deflagration and detonation (fig. 2.3). The combustion is a redox reaction initiated by the input of activation energy, mostly governed by thermal exchanges. The kinetic of this kind of chemical reaction was described by the Arrhenius equation (1889) [Lakner, 2010]. The thermal theory of combustion was described by Semyonov (1934) and Frank-Kamenetskii (1947) [in Lakner, 2010] relying on the species evolution of oxidizer, combustive and heat transfers between them and their environment. When the kinetic of the reaction is being carried away, it accelerates products of reaction and the combustion regime evolves as a deflagration. Under certain conditions, the reaction can be accelerated again towards a supersonic flow and a Deflagration to Detonation Transition (DDT) can occur.

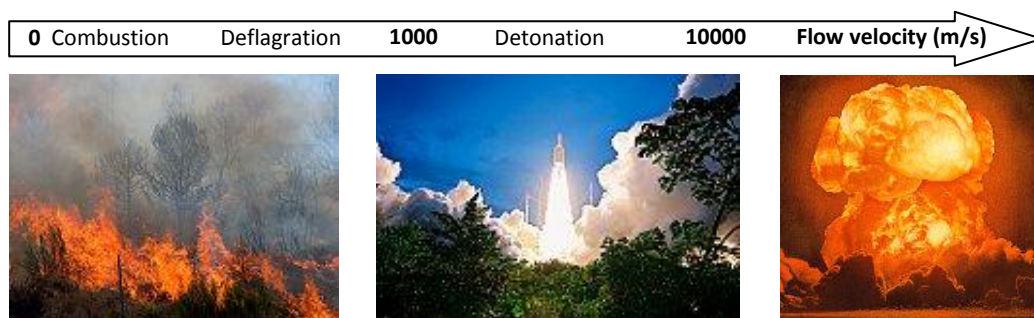


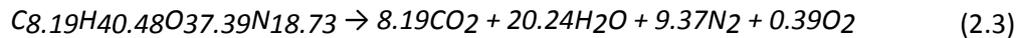
Figure 2.3: Decomposition regimes, left, combustion – center, deflagration – right, detonation.

Scheme of decomposition for high explosives

The composition of detonation products is usually computed by thermo-chemical codes like Cheetah or *Explo5*® when accessible. For high explosives composed of $C_xH_yO_zN_w$, including mixtures, one can adopt as a first approach the following decomposition scheme:

- All N compounds are transformed in N_2
- All H compounds are transformed in H_2O
- All O left are transformed in CO
- All O left, if any, are transformed in CO_2
- There are always traces of NO_x (less than 1%)

Example: If one considers 1 kg of the explosive mixture determined in table 2, the global decomposition mechanism of the energetic material will be (2.3):



➤ *Exercise 3: Determine the composition of detonation products of Composition B.*

2.6 Hess's law

Hess's law declares that the variation of enthalpy in a chemical reaction, at constant pressure, does not depend on the pathway between the initial and final state.

This allows considering respectively reactants and products at a standard initial and final state, if possible known (available in a thermodynamic data table, for example [Meyer, 2007]), as specified in equation (2.4). This variation of enthalpy is named heat of reaction. For combustion, it is considered as being the heat of combustion and for detonation, the heat of detonation.

$$\Delta_r H_{deto} = \Delta H_f^0(\text{products}) - \Delta H_f^0(\text{Reactants}) = -Q_{detonation} \quad (2.4)$$

The Hess's law can be extended to the energy conservation (for constant volume transformations). It is considered that the energy of formation of a simple constituent, like N_2 , is null.

Example: The detonation energy of the solid explosive presented in table 2 is determined with energies of formation given in table 3 [Meyer, 2007]:

Det. Prod.	E_f^0 kcal/mol	Nb moles	E_f^0 (prod)
CO ₂	-94.05	8.19	-770.27
H ₂ O vap.	-57.50	20.24	-1163.80
Total			-1934.1

Table 3: Energies of formation of detonation products in reaction (2.3) [Meyer, 2007].

Thus: $Q_{Deto} = -\Delta E_{Deto} = E_f^0(\text{prod}) - E_f^0(\text{reactants}) = -767.9 - (-1934.1) = 1167 \text{ kcal/kg of explosive}$

Where $E_f^0(\text{reactant})$ has been determined in paragraph 2.2 and $E_f^0(\text{prod})$ is determined in table 3.

Remark: It is important to note that the detonation properties of a high explosive (the Chapman-Jouguet state P_{CJ} , D_{CJ} ...) will strongly depend on its heat of detonation. They can be approximate by empirical formulations that can be found for example in [Kamlet, 1968]. This will also determine the key parameters of a blast wave generated in air by the aerial detonation of a high explosive.

➤ *Exercise 4: Determine the Energy of detonation products of composition B.*

3. Blast waves

A blast wave is the thermo-mechanical consequence of an explosion in a compressible media.

An explosion is a high rate deliberation of energy than can be mechanical (rupture of a pressurised tank), chemical (high explosive) or atomic (nuclear weapons). In the following chapters, only chemical explosions will be considered.

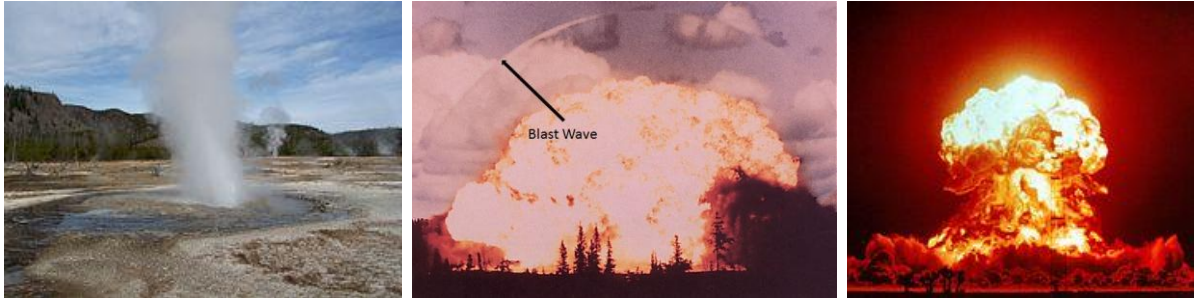


Figure 3.1: Left, pneumatic explosion occurring in a geyser – center, chemical explosion a conventional weapon – right, thermo-nuclear explosion of the 15 MT H bomb castle Bravo -1954. (All pictures are taken from Wikipedia and are free of right).

Blast wave profile

A blast wave can be considered as a shock wave generated by an explosion that propagates in a fluid compressible medium (mostly in air). In the case of a spherical explosive shocks in air, it is provoked by the transmission of the detonation wave in a shock wave propagating in the compressible fluid. Indeed, the detonation products at high pressure, density and temperature, are pushed outwards the initial place of the charge and compress the surrounding air while propagating. It results in a steep rising front on the pressure versus time records $P(t)$ (fig. 3.2).

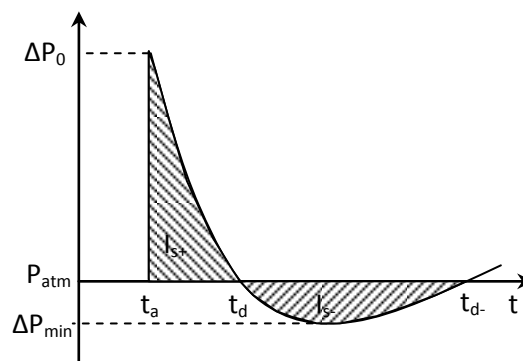


Figure 3.2: Blast wave profile and parameters.

The parameters of the blast wave are the time of arrival at the observation point t_a , the maximum overpressure ΔP_0 , the positive impulse I_{s+} , its duration $(t_d - t_a)$, the minimal pressure ΔP_{min} and the negative impulse I_{s-} and the duration of the negative impulse t_{d-} .

3.2 The release

The shock pressure within the detonation products at the break out in air is about the Chapman-Jouguet pressure PCJ, that is to say, of the order of 21 GPa for the TNT [Dobratz, 1985]. 1 mm after having left the charge of 1kg of TNT, the shock pressure has decreased down to about 48 MPa ! This

breathhtakingly fast drop is a consequence of the strong shock impedance mismatch between detonation products and the surrounding air. Behind this shock front, an isentropic release runs backwards the shock front at a local sonic velocity, which is even faster than the shock wave itself. Release waves catch-up the shock front and interact with it, resulting in a hydrodynamic damping. While propagating outwards, the shock energy is spread over an increasing spherical surface, what also diminish the shock amplitude. The release pressure profile behind the shock front is known as the Taylor release [Taylor, 1954]. Some analytical models have been proposed to describe the blast wave [Taylor 1950, Sakurai 1953, Bach 1970]. The simplest analytical approach for describing a blast wave in free field remains the Friedlander equation (3.1) at a given distance Z from the centre of the explosion:

$$P(t) = P_{atm} + \Delta P_0(Z) \left(1 - \frac{t - t_a(Z)}{t_d(Z)} \right) e^{-\frac{\alpha(Z)(t - t_a(Z))}{t_d(Z)}} H(t - t_a(Z)) \quad (3.1)$$

With H the Heaviside function that is 1 if $t > t_a$ and 0 otherwise. α is a shape parameter given in a table [Kinney, 1985] or to be determined.

The negative impulse

After the rapid spherical expansion of the shock, all the gas included in the sphere of the shock has been pushed against the shock front, making a depression. This depression also propagates behind the front and gives a negative impulse. Its parameters are given in [Kinney 1985]. This suction brings back on the centre of explosion, some materials that surround the charge.

3.3 The fireball

As seen in paragraph 2.3, some explosives are under oxygenated, their detonation products burn with the oxygen of air. Hence, a fireball appears and emits thermal effects around. Sensors can be affected in close range. Some experimental approaches propose evolution laws of the maximum radius r of the fireball versus the explosive charge mass W . Among them, one can find a simple formulation (3.2), obtained with TNT charges ranging from 1 kg to 1000 kg [Gross, 2007]:

$$r = aW^b \quad (3.2)$$

with $a=278 \pm 74 \text{ cm.kg}^b$ and $b=0.33 \pm 0.05$

3.4 The mixing layer

In free air detonation of high explosives, detonation products of under oxygenated explosives can burn with oxygen of air. This is called “afterburning” and this phenomenon can bring to the blast wave a considerable energy (about + 250% for the TNT).

Turbulent mixing in fireballs has been described by Kuhl [Bowen, 1996]. He considered a PBX-9404 explosive, supposed to be oxygen balanced (no afterburning). He gave some quantitative results about the mixing layer of detonation products with surrounding air. He could distinguish four phases that are:

- The blast front that strongly blows away detonation products.
- The implosion phase which is the consequences inertial effects of the heated air in ambient surrounding air. It provokes a gas implosion that stretches the inner boundary of the mixing region.
- Once the implosion achieved, the imploded air emits a secondary shock wave (similar to what happens in underwater explosions [Cole 1948]). This is the "Re-shock" phase. When the secondary shock interacts with mixing layers, it re accelerates them, marking a singularity on the layer evolution.
- The asymptotic mixing phase where the fireball size remains quasi-constant.

These phases are gathered on figure 3.3 that shows a qualitative space-time diagram of high explosive driven blast waves.

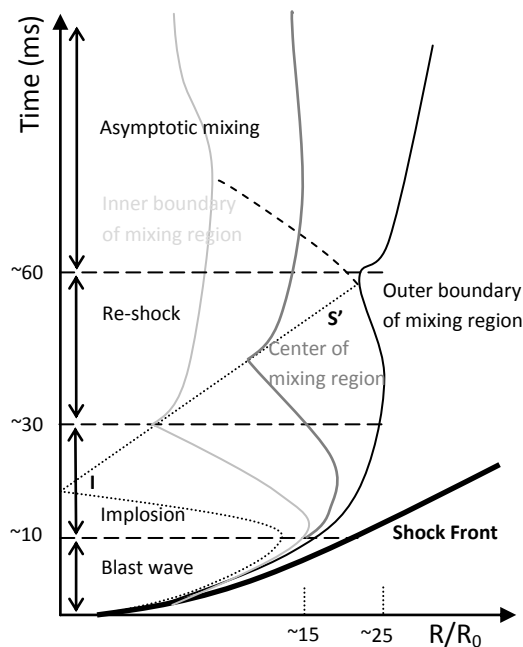


Figure 3.3: Wave diagram of high explosive driven blast wave.

4. Similitude laws

Vaschy Buckingham theorem

The Vaschy-Buckingham theorem, also named theorem Π , states that for an equation of n physical variables that can be expressed in k dimensions, there is an equivalent formulation involving a set of $p = n - k$ dimensionless parameters deduced from these physical variables.

4.1 Scaling laws (Hopkinson-Cranz)

Let's consider two experiments of aerial detonation of a spherical charge that are respectively situation A and situation B (fig. 4.1). In situation A, the charge is spherical with a Weight W_1 , diameter d_1 . It generates an overpressure ΔP_{01} at a distance R_1 of the centre of the explosion. In situation B, the charge is also spherical, with a diameter $d_2=k*d_1$, and generates an overpressure ΔP_{02} at a distance R_2 of the centre of the explosion.

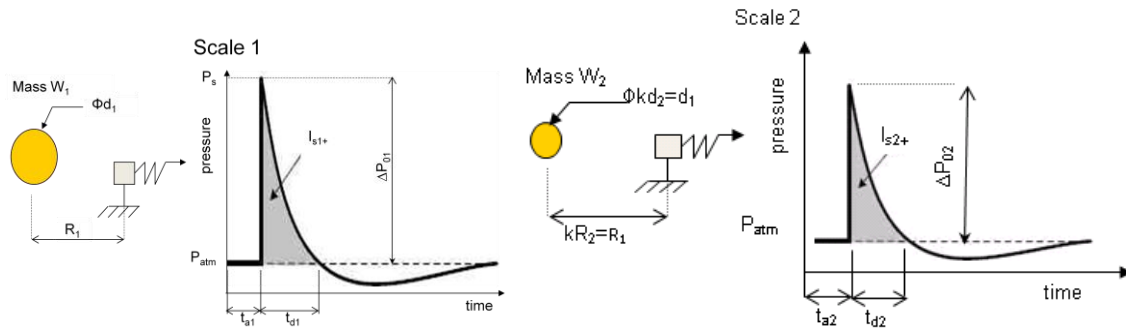


Figure 4.1: Two experiments of aerial detonation of a spherical charge. Situation B is scaled from Situation A with a factor k .

The problem can be defined by the following variables and their units: E [$\text{kg}\cdot\text{m}^2\cdot\text{s}^{-2}$] is the detonation energy, W [kg] is the weight of the charge of diameter d [m] inducing a blast wave of pressure P [$\text{kg}\cdot\text{m}^{-1}\cdot\text{s}^{-2}$] at a distance R [m] from the centre of the charge.

According to the Vaschy-Buckingham theorem, there is a function of $n=5$ variables (W,P,E,R,d) depending on $k=3$ dimensions ($\text{kg}, \text{m}, \text{s}$) satisfying: $f(W,P,E,R,d)=0$ and there are $p=n-k=2$ dimensionless parameters that can be used for similitude study. They can be found by decomposing variables in the unit base, as shown in table 4, in which positive and negative powers are placed in the unit base.

	<i>kg</i>	<i>m</i>	<i>s</i>
<i>W</i>	1	0	0
<i>P</i>	1	-1	-2
<i>E</i>	1	2	-2
<i>d</i>	0	1	0
<i>R</i>	0	1	0

Table 4: decomposition of the 5 variables describing the explosion, in a base of 3 dimensions.

One can search for an obvious dimensionless number or can find it by the Gauss method applied to the matrix in table 4.

One can find the following dimensionless form (4.1):

$$f\left(\frac{d}{R}, \frac{E}{PR^3}\right) = 0 \quad \text{And} \quad \pi = \frac{E}{PR^3} \quad (4.1)$$

It means that situation A and situation B are in similitude implies (4.2) :

$$\pi_1 = \pi_2 \Leftrightarrow \frac{E_1}{\Delta P_{01} R_1^3} = \frac{E_2}{\Delta P_{02} R_2^3} \Leftrightarrow \frac{d_1}{R_1} = \frac{d_2}{R_2} \quad (4.2)$$

However, $W_1=(1/k^3).W_2$ as $E_1=k.E_2$ and $d_1=k.d_2$ thus $\Delta P_{01} = \Delta P_{02}$

In similitude, the pressure is not affected by the scale factor!

The reduced distance Z can be then introduced as (4.3):

$$Z = \frac{R}{E^{\frac{1}{3}}} \quad \text{Or} \quad Z = \frac{R}{W^{\frac{1}{3}}} \quad (4.3)$$

4.2 Diagrams

Experimental data obtained on blast wave experiments have been gathered and plotted versus the reduced distance Z defined by expression (4.3). An example taken from the UFC 3-340-2 is plotted in figure 4.2. Pso is the overpressure and Z is taken from the centre of the TNT spherical charge.

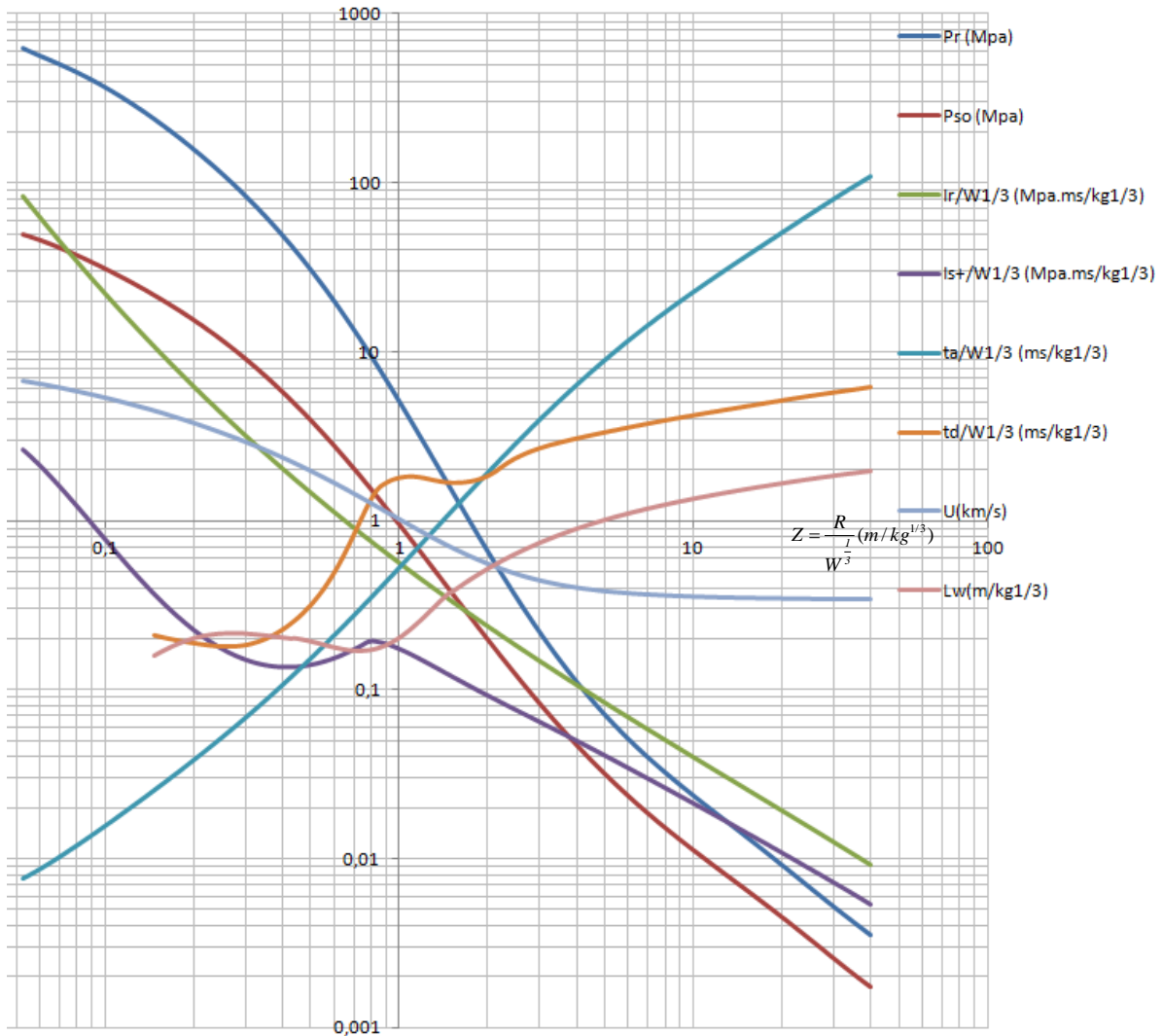


Figure 4.2 : blast wave parameters versus scaled distance $Z=R/W^{1/3}$ in $m/Kg^{1/3}$ for 1kg of TNT spherical charge.

[UFC 3-340-2]. Values are given in table A.1 in annexe 1.

This set of parameters does not specifies the value α given in expression (3.1). Some empirical expressions can provide an analytic fit of these curves (4.4-4.6) [Kinney, 1985]. The overpressure is given by expression (4.4):

$$\Delta P_0 = \frac{808 \left[I + \left(\frac{Z}{4.5} \right)^2 \right]}{\sqrt{I + \left(\frac{Z}{0.048} \right)^2} \sqrt{I + \left(\frac{Z}{0.32} \right)^2} \sqrt{I + \left(\frac{Z}{1.35} \right)^2}} P_{atm} \quad (4.4)$$

The positive impulsion I_{s+} and the time of duration ($t_d^- - t_d^+$) are respectively given by expressions (3.7) and (3.8):

$$I_{s+} = \frac{0.067 \sqrt{I + \left(\frac{Z}{0.23} \right)^4}}{Z^2 \sqrt[3]{I + \left(\frac{Z}{1.55} \right)^3}} \quad (4.5), \quad \frac{t_d^-}{W^{\frac{1}{3}}} = \frac{980 \left[I + \left(\frac{Z}{0.54} \right)^{10} \right]}{\left[I + \left(\frac{Z}{0.02} \right)^3 \right] \left[I + \left(\frac{Z}{0.74} \right)^6 \right] \sqrt{I + \left(\frac{Z}{6.9} \right)^2}} \quad (4.6)$$

The parameters for the negative phase, respectively the minimal pressure ΔP_{min} , the negative pulse duration t_d^- and the negative impulsion I_{s-} are given by respective relations (4.7-4.9):

$$\Delta P_{min} = -\frac{0.35}{Z} \quad (4.7), \quad t^- = 1.25 W^{\frac{1}{3}} \quad (4.8), \quad I_{s-} = I_{s+} \left[I - \frac{I}{2Z} \right] \quad (4.9)$$

Remarks:

- Some other can be of interest, among them, [Baker, 2012], [Brode, 1955], [Henrych, 1979], [Kingery, 1966].
- One must keep in mind that data is in log-log scale and thus, a small error of reading will have a greater impact on the actual value.
- These given values only concern blast wave generated by spherical charges of TNT and will not be suitable for other charge geometries or high explosives !

➤ *Exercise 5: What will be the blast parameters at 1m from the center of a spherical charge of TNT ?*

5. TNT equivalent

5.1 A delicate concept

In order to use figure 4.2 with other high explosives, it is necessary to consider a mass TNT equivalent W_{EqTNT} of the concerned explosive. This step is delicate and an error of appreciation of the input data (the weight of explosive) may have some incidences on the searched result (pressure, impulse, ...).

5.1.1 Heat of detonations ratio

One of the most relevant ways is to multiply the effective mass of high explosive by the ratio of the heats of detonation of the explosive $Q_D(\text{explosive})$ by the one of the TNT, $Q_D(\text{TNT})$, as suggested by UFC-3-340-2 (5.1). Q_D can be calculated by the Hess’s law (paragraph 2.6) either by considering the enthalpies or the energies of reaction:

$$W_{EqTNT} = \frac{Q_D(\text{explosive})}{Q_D(\text{TNT})} W_{\text{explosive}} \quad (5.1)$$

It is often considered that the heat of detonation of 1kg of TNT is about 1Mcal (4,18 MJ).

5.1.2 Maximum pressure or impulse ratio

These considerations suppose to know the explosive formula and depend on the adopted scheme of decomposition for calculating the heat of detonation. This is why it is sometimes more convenient to consider the ratio of overpressure of the high explosive $\Delta P_0 \text{exp}$ by the one of TNT, $\Delta P_0 \text{TNT}$ (5.2) – or the ratio of positive impulses $I_{s+} \text{Explosive}$ by $I_{s+} \text{TNT}$ (5.3) – measured at a given distance:

$$W_{EqTNT} = \frac{\Delta P_0(\text{explosive})}{\Delta P_0(\text{TNT})} W_{\text{explosive}} \quad (5.2)$$

$$W_{EqTNT} = \frac{I_{s+}(\text{explosive})}{I_{s+}(\text{TNT})} W_{\text{explosive}} \quad (5.3)$$

These both methods not only require preliminary experiments but also are dependent on the distance at which the overpressure – or the impulse – is chosen.

5.1.3 Berthelot Method (1892)

The Berthelot method states that the TNT equivalent, in %, can be expressed as (5.4):

$$\text{TNT Equivalent (\%)} = 840 \Delta n (-\Delta_d H(\text{explosive})) / M_{\text{EXP}}^2 \quad (5.4)$$

Where:

Δn is the number of moles of generated gases by the detonation of one mole of explosive.

$-\Delta_d H(\text{explosive})$ is the heat of detonation in kJ/mol.

M_{EXP} is the Molecular weight of the Explosive (g/mol)

5.1.4 Cooper’s method

Cooper [Cooper, 1996] proposed a practical formula giving the equivalent TNT of a high explosive from its detonation velocity (5.5):

$$W_{eqTNT} = \frac{D_{\text{explosive}}^2}{D_{\text{TNT}}^2} \quad (5.5)$$

Table 5 gives a comparison of Berthelot and Cooper’s methods [Locking, 2011]. Berthelot’s Method seems to provide more accurate values excepted for Pentolite. Although simple, these methods must be handled with care.

Explosive	Experimental value	Berthelot method	Difference in %	Cooper method	Difference in %
Ammonitrate Picrat	85	87	2	97	14
HBX-3	116	110	-5	100	-14
Pentolite 50/50	105	156	49	115	10
Torpex	122	118	3	120	-2
Tritonal	110	89	-19	90	-18

Table 5: Comparison of TNT equivalents determined experimentally and respectively by Berthelot and Cooper's methods.

5.1.5 Remarks:

- In the calculation of the TNT equivalency by heats of detonation, the post-detonation combustion of detonation products with surrounding air (afterburning occurring for under oxygenate explosives), is not considered but will have an effects for short range analysis, especially in confined environment. A method for determining the TNT equivalency including the effect of afterburning is given in the UFC-3-340-2, paragraph 2-14.3.3.
- It will be then fundamental to mention which of these methods has been used for calculating the TNT equivalency.
- It may be relevant to major by 20% the mass of TNT estimated for safety reasons. That will consider eventual errors due to the log-log appreciation or the exactitude of the decomposition scheme, or the approximate sphericity of the charge, uncertainties on the explosives ...

➤ *Exercise 6: Calculate the TNT equivalent in heat of detonation of the composition B.*

5.2 The reference TNT

Although the TNT, or *2,4,6-Trinitrotoluene*, has become a reference for high explosives, one should keep in mind some important considerations.

First of all, there are three isomers for the TNT: *2,3,4-trinitrotoluene*, *2,3,5-trinitrotoluene* and *2,3,6-trinitrotoluene*. Each of them has its own scheme of decomposition leading to different heat of detonation.

Then, the detonation pressure of the TNT depends strongly of its initial density ρ_{0TNT} [Cooper, 1996]. So it is important to specify the initial density of the TNT considered. It is suggested to adopt Dobratz's TNT as the reference TNT [Dobratz, 1985]. Physical data is given in table 6: coefficients A , B , R_1 , R_2 , w and E_0 is the JWL coefficients parameters set and is not discussed in this chapter.

ρ_0 (g/cm ³)	P_{C1} (GPa)	D_{C1} (m/s)	A (GPa)	B (GPa)	R_1	R_2	w	E_0 (MJ/m ³)
1,63	21	6930	371,21	3,23	4,15	0,95	0,3	7000

Table 6: Dobratz's TNT parameters as the reference TNT [Dobratz, 1985].

Remark: For explosives considered at a density that differs than the one of its reference, it is possible to estimate detonation state (P_{CJ} , D_{CJ} , ΔrH) at given density from the known one. These methods are proposed by Kamlett & Jacobs [Kamlett, 1968], Hardesty & Kenedy [Hardesty, 1977] and Keshavartz [Keshavartz, 2002].

5.3 Charge geometry

Explosive charges of spherical shape are of interest in detonics experiments because of the homogeneous pressure fields that are generated by their aerial detonation. However, they are not really representative of an accidental explosion of explosive heap neither of the detonation of a warhead or a mine.

When the charge geometry differ from the spherical one, data presented in paragraph 4.3 are not longer acceptable, especially in short range.

Data for hemispherical, cylindrical and orthorhombic charges can be found in the UFC-3-340-2 and are usable for specified explosives and charge geometries. Some authors have tried to find analytical solutions of the pressure field generated by the detonation of a long cylinder (explosive wire) [Plooster, 1968, 1982]. He concluded that the position of the detonator and the L/D ratio play an important role in the blast propagation in short range. Katselis [Katselis, 2001] and Wu [Wu, 2010] gave a description of the blast wave in a polar diagram and concluded that the maximum pressure around the charge depended on the ignition side. When placed at the center of the charge, the field pressure was observed as to be symmetrical. Ismail et al [Ismail, 1993] introduced the "bridge wave" that join the blast front from the curved side, to the blast front from flat ends (fig. 5.1). Detonation products, from the curved side, follow a toric shape, while at flat ends, they take the form of arrows along the cylinder axis. There are almost no traces between these two shapes. Actually, the blast measurements in these "dead angles" indicate lower pressures that compose the bridge wave, making the blast front continuous from the cylinder axis direction to the radial direction (fig. 5.1, right)

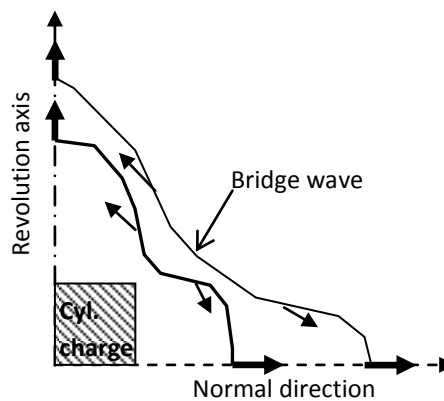


Figure 5.1: left, detonation of a spherical charge, right: bridge wave [Simoens, 2012].

Figure 5.2 shows polar diagram at 110 cm of charges made of explosive emulsion (i.e. maximum pressure on a propagation angle in the median plane) [Péchoux, 2010]. The dead angle clearly appears. It can be noticed that the position of the detonator has a strong effect in close range.

At a longer range, hydrodynamic phenomena tend to homogenize the blast front and at a certain distance, the blast wave has become homogenous and equivalent to the one of a spherical charge. The length to diameter ratio L/D plays a major role in the distance taken by the blast to be homogeneous. Simoens et al [Simoens, 2012] proposed a parametric study of the blast generated for different L/D ratios, by numerical simulation validated by some experimental cases. They studied explosive emulsions encapsulated in cylinders for L/D=1 and L/D=8.3. They observed the shape effect

of cylindrical explosive charges to be noticeable on the center plane, up to an influence distance, which depends on the charge shape. In the case of the “long” cylinder ($L/D=8.3$), shape effects have been observed up to a reduced distance above which, the overpressure and the impulse are below the ones of the spherical charge of the same mass of explosive. This shape effect can lead to the use of a lower amount of explosive in a different shape with the same effect.

The casing of the charge could be suspected as playing a role on the blast wave. However, as mentioned in the UFC-3-340-2, a review on the subject has showed that the casing effect could be neglected.

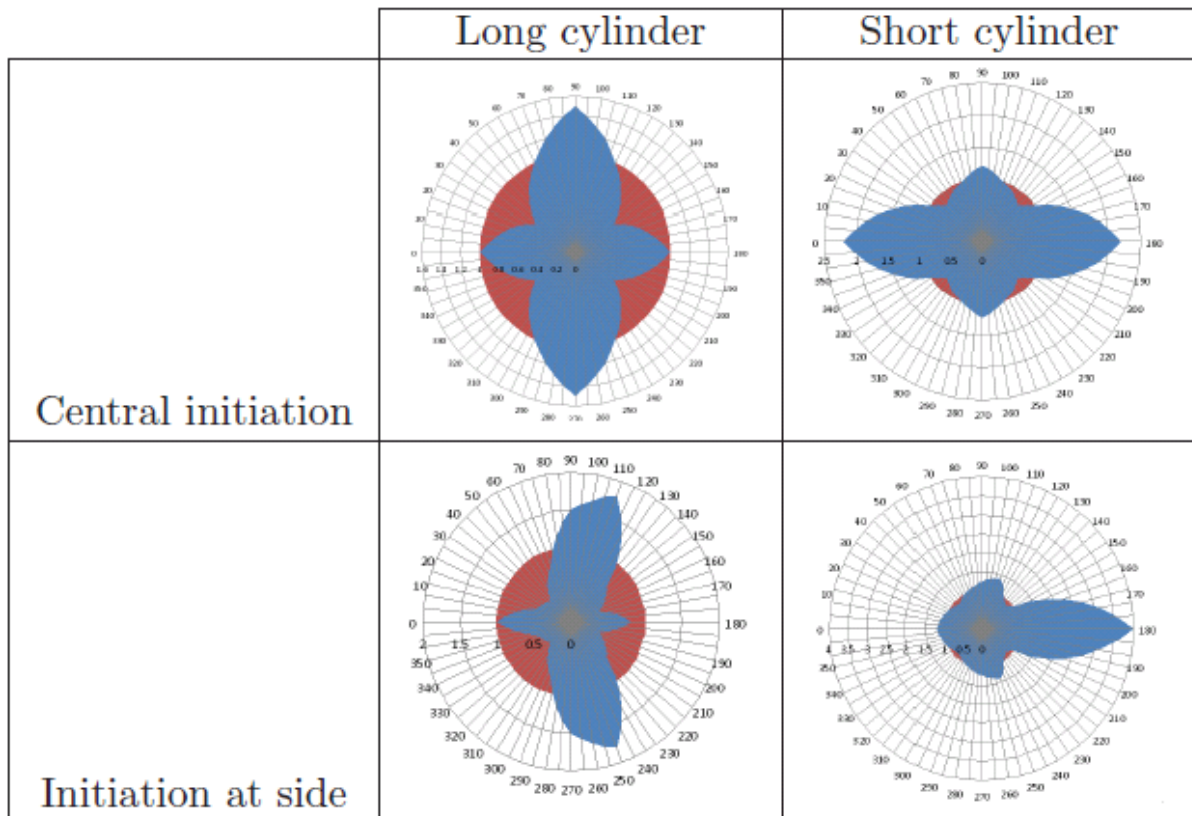


Figure 5.2: Polar diagram of peak pressure recorded at 110 cm of a cylindrical charge depending on its initiation, compared with a spherical charge (red). Long and short cylinders are respectively $L/D=8.3$ and 1.

5.4 Some TNT equivalents

TNT equivalents have been gathered from the literature. In any case, their use must be used carefully and the method for determining the TNT equivalent must be specified. Table 7 is extracted from [Locking, 2011] and gives some TNT equivalents based on pressure and impulse ratios, obtained by experiments, for various explosives. The range of validity is also specified.

Explosive	Density g/cm ³	Equivalent for Pressure peak	Equivalent for positive impulse	Range of validity
ANFO 94/6		0.87	0.87	0.03-6.9
Comp B	1.65	1.11	0.98	0.03-0.35
Comp B	1.65	1.2	1.3	0.69-6.9
cyclotol (RDX/TNT) 70/30	1.73	1.14	1.09	0.03-0.35

Cyclotol (RDX/TNT) 75/25	1.71	1.11	1.26	
cyclotol 60/40	1.74	1.04	1.16	
H6	1.76	1.38	1.15	
HBX-1	1.76	1.117	1.16	0.03-0.14
HBX-3	1.85	1.14	0.97	0.03-0.17
HMX		1.25	1.25	
Nitromethan		1	1	
Octolite (HMX/TNT) 70/30	1.14	1.09	1.09	0.01-0.3
Octolite (HMX/TNT) 75/25	1.81	1.02	1.06	
PBX 9404	1.81	1.13	1.13	0.03-0.69
PBX 9404	1.81	1.7	1.7	0.69-6.90
PBX 9502	1.89	1	1	
PBX N107	1.64	1.05	1.05	
PBX N109	1.67	1.05	1.05	
Pentolite	1.68	1.38	1.14	0.03-4.14
PETN	1.77	1.27	1.27	0.03-0.69
RDX		1.1	1.1	
TATB		1	1	
TNT	1.63	1	1	
Torpex	1.85	1.23	1.28	0.01-0.3
Tritonal 80/20	1.72	1.07	0.95	0.03-0.69

Table 7: TNT equivalents obtained by blast experiments [Locking, 2011]

6. Blast measurement

6.1 Physics of sensors

Dynamic pressure measurement requires not only fast response time, with high bandwidth but also the ability of measuring small pressure changes at high static pressure levels in harsh environment. This can be possible by the use of the piezoelectric material encapsulated in an engineered rugged solid state device. Piezoelectric materials are most of the time Quartz, PZT, Tourmaline or ceramics. The piezoelectricity is defined as a dual effect of the electrical behavior of the material combined with its mechanical behavior. The electrical behavior is described by a relation between its electric charge density displacement δ versus the strength of the electric field Σ (6.1):

$$\delta = \eta \Sigma \quad (6.1)$$

Where η is the electric permittivity.

The mechanical behavior is given by the Hook law between stress σ and the young modulus E (6.2):

$$\sigma = E \varepsilon \quad (6.2)$$

Where ε is the mechanical strain.

Both equations (6.1) and (6.2) can be coupled in the strain-charge system which will not be explicated in this chapter.

The piezoelectric material is encapsulated in a metallic shell, coated with a diaphragm (fig. 6.1). Charges are collected by a wire and the housing is connected to the electrical earth in order to offer an electromagnetic shielding. The insulation resistance between signal and shielding is generally greater than 10^{12} Ohms.

It is also important to have an idea of the blast wave thickness versus the sensitive area of the sensor, as the signal delivered by the sensor will be the electric charges given by the excitation of the overall area.

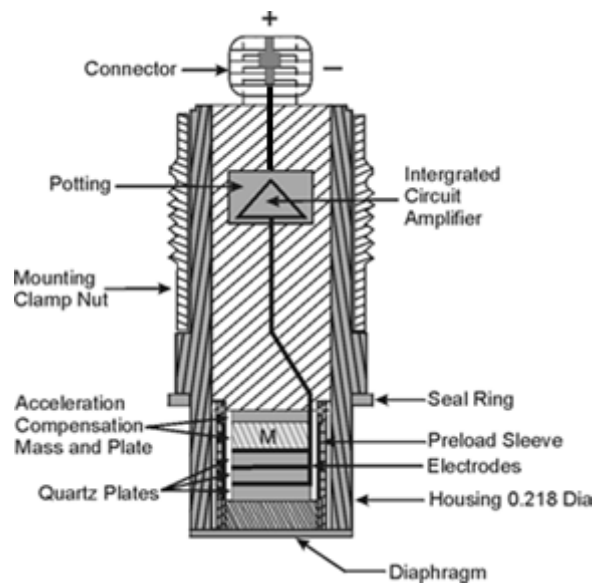


Figure 6.1: Cross section of a piezoelectric sensor for pressure measurement. [PCB®]

6.2 Acquisition chain

6.2.1 Sensor electronic adaptation

At least two technologies are available on the market: charge mode sensors and Integrated Electronics Piezo Electric (IEPE).

Charge mode sensors are usually high output impedance and can operate above 500°C. The signal, obtained by the stressed piezoelectric material, must be converted by a charge amplifier in voltage per mechanical unit. It is crucial to preserve the signal from radio frequency and electromagnetic interferences by ensuring connexions and signal routing with low noise and shielded cables. Moreover, according to the law of electrostatics, the voltage signal will depend on the sensing charge divided by the capacitance of the acquisition line. However, this capacitance includes the cable capacitance, that is to say the calibration of the sensor is given for a certain length of wire. If this length is modified, the sensor calibration has to be done again.

IEPE sensors are the fruit of recent developments in integrated circuit technology for signal conditioning. They include a built-in microelectronic charge amplifier that result in a low impedance output when coupled with a signal conditioner. They have to be powered by a constant current source in order to have accurate measurements and an excitation voltage between 18 to 30 V. This technology offers the advantage to not depend on the cable length or capacitance for frequencies below 10 kHz; it can be used with standard coaxial cable and are directly pluggable on acquisition instruments. For higher frequencies and long cable (>30m) the signal may be distorted. The maximal signal frequency f_{max} (in Hz) that can be measured with a given cable length is determined by relation (6.3):

$$f_{max} = \frac{10^9}{2\pi CV(I_c - 1)} \quad (6.3)$$

With C the cable capacitance, function of its length, V the maximum signal voltage, I_c the constant current from the conditioner in mA.

A graphical method, using figure 11 allows determining the maximal frequency that can be recorded by the IEPE sensor, knowing peak signal, cable capacitance and supplied constant current. For instance, a 20 m cable having a 100 pF/m capacitance will have a total capacitance of 2000 pF. If the sensor operates on a 50 Ohm input channel, one can assume its maximum voltage to be 5V. One can also assume that the constant current signal conditioner to be 2 mA. The ratio on the ordinate axis is equal to 5 and the intersection with the oblique line of 2000 pF is about $f_{max}=16$ kHz. It is recommended to use a safety factor of 2 for the determination of f_{max} .

In general, one must care that the discharge time constant (DTC), equal to the input impedance times the coupling capacitance, must be greater than the recorded signal time. In DC coupling, the DTC will be fixed by the sensor constitution. In AC coupling, the DTC may be a limiting factor for low frequency measurements. For instance, if one considers a AC coupling conditioner with a 8μF coupling capacitor plugged with a 1 MOhm input impedance oscilloscope, the coupling time constant will be 10 s. It is recommended to have a coupling time constant ten times larger than the sensor time constant.

6.2.2 Sampling rate

The sampling rate has to follow the Shannon theorem that states the sampling rate must be at least twice as much as the maximum signal frequency; otherwise, the recorded data may miss physical values (fig. 6.2).

The maximum signal frequency must be lower than the upper bandwidth of the sensor; otherwise, the rise of the signal may be altered (fig. 6.3).

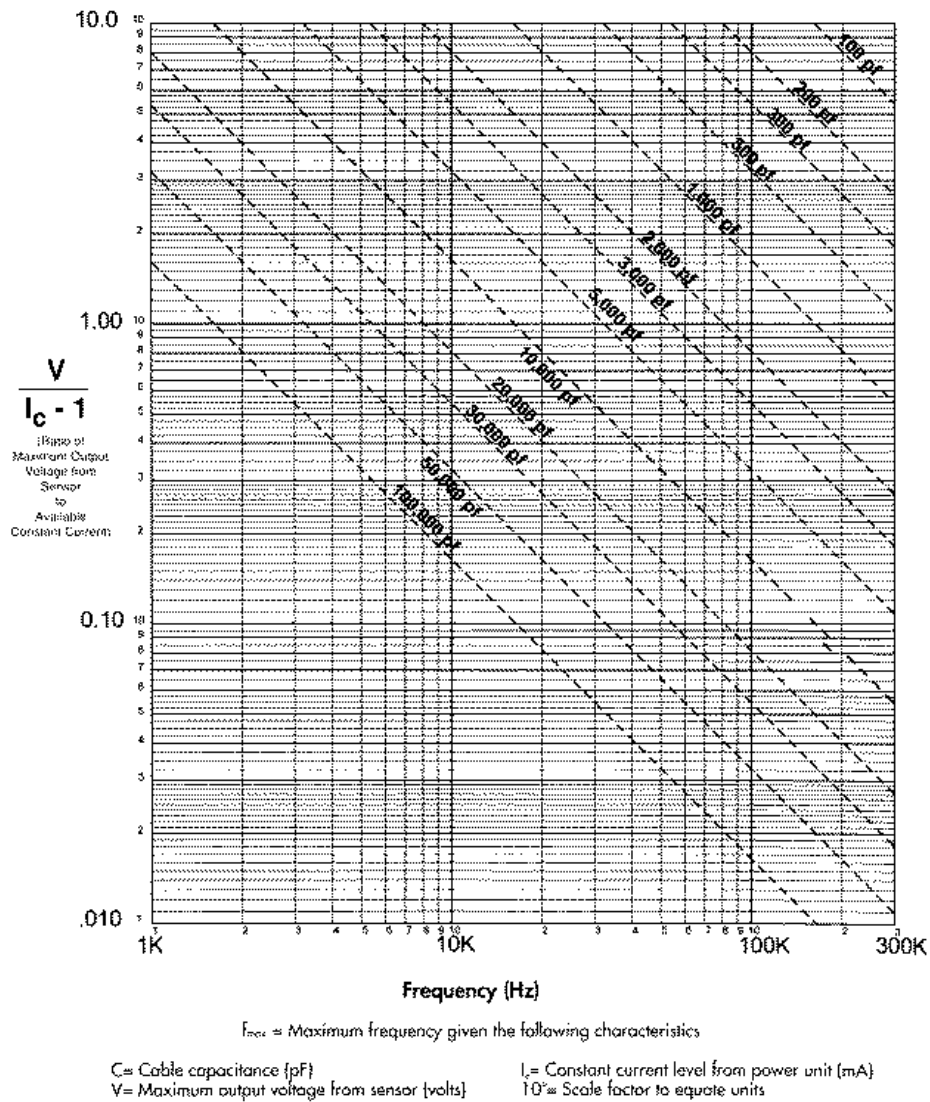


Figure 6.2: Nomograph for maximal frequency determination. [PCB®]

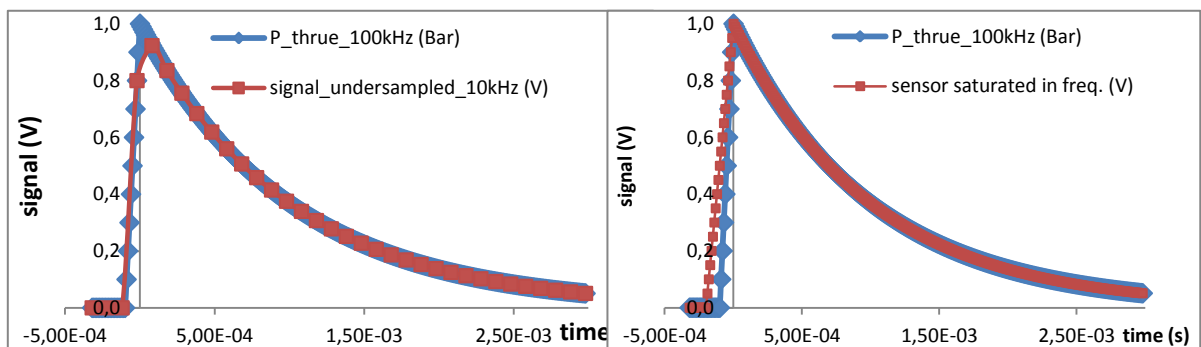


Figure 6.3: Left: an under sampled signal (dashed) may not be representative of the real signal (full). Right: a maximum bandwidth lower than the maximum signal frequency (dot) may not be representative of the real signal.

6.2 Sensor mounting

6.2.1 Flush

In order to measure the incident pressure of the air blast, the blast wave must not interact with any part of the sensor mounting. The flush mounting will be then preferred (fig. 6.4). One must also pay attention to the ground shock that propagates faster than the air blast and can reach the sensor mount before the blast. Side loading of the sensor may also disturb the signal output; an O-ring mount could minimize this effect.

Sometimes, sensor mounting presents a recess more or less important. It may have an influence on the measured pressure. Figure 6.5 shows a blast wave – mount interaction. Pressure is plotted on the sensing membrane and figure 6.5, right shows that discrepancies are actually induced by the recess.

Thermal shock may also disturb the signal because of thermal stresses generated on the piezoelectric material encapsulated in the sensor. This effect can be limited by coating the sensing area of the sensor by silicone grease for air blast experiments, or a vinyl tape in shock tube.

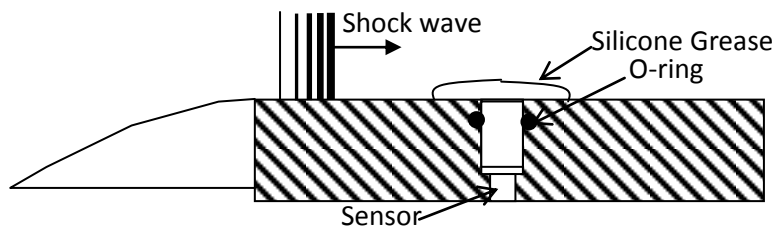


Figure 6.4: Flush mounting of a sensor, in shock-tube wall or blade or pencil mount for blast measurement.

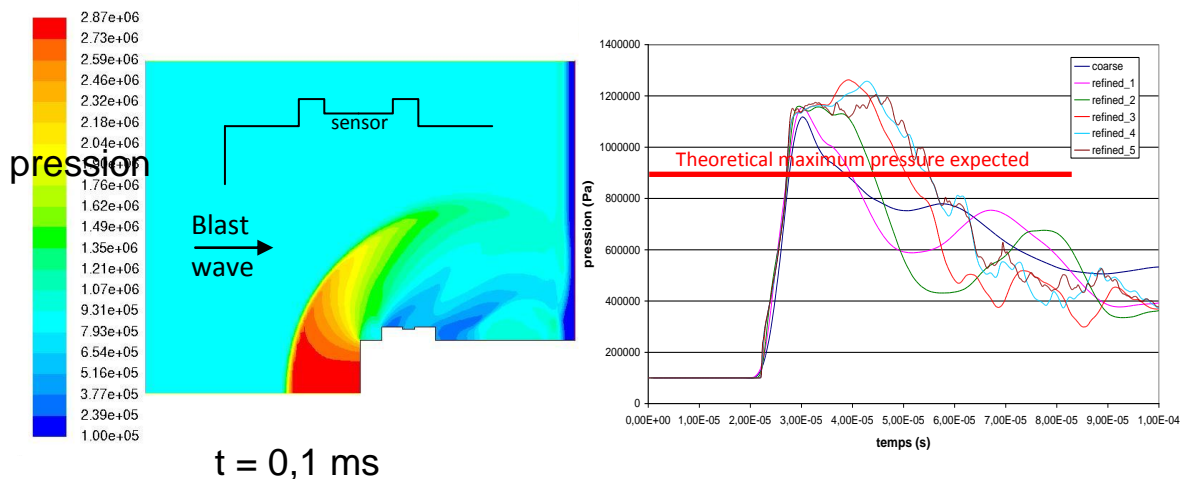


Figure 6.5: influence of a slight recess of the sensor mount on the pressure measurement. Left: CFD simulation of the blast – mount interaction. Right: pressure amplitude versus mesh refinement.

6.2.2 Pencil blast pointing

In order to measure blast wave incident pressures, the sensor is mounted in an aerodynamic pencil-like shape (fig. 6.4). The pencil has obviously to point towards the charge centre. Two angles have to be adjusted. This can be simplified by using a disc instead of a pencil. A small deflection may perturb the blast wave and lead to incorrect measurements. Experimental results showing the effect of intentional pencil deflections with exposed gauges and non exposed gauges are shown in figure

6.6 and clearly lead to discrepancies that might be important once taken out of the log-log diagram [Bailleau, 2013].

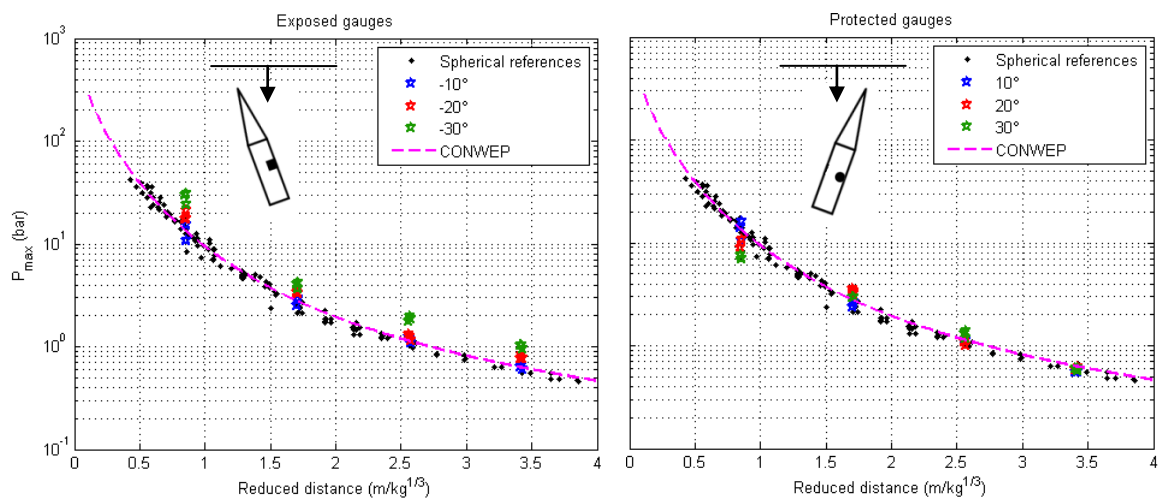


Figure 6.6: Influence of the deflection angle on the pressure measurement [Bailleau, 2013].

6.3 Signal exploitation

Values presented on figure 6.6 can be deduced from pressure sensor records. In order to have an accurate measurement of the time of arrival – time between the detonation of the detonator and the blast wave that hits of the sensor – it is necessary to trig the acquisition chain with the detonator by using a suitable trigger device (i.e. ionization probe, optical fibre, exploded wire, ...). Then, before reading the maximum pressure, it is necessary to check carefully if the rising front is constituted of several samples (paragraph 6.2). Sometimes an overshoot can be observed and may be the effect of the ground shock that propagates in solid (faster than the air shock) and thus, may pass in the sensor mount. But it can also be a “ringing” in the piezoelectric material submitted to a step load. Figure 6.7 taken from [Guerke, 1990] summarizes some features that can be observed in pressure records.

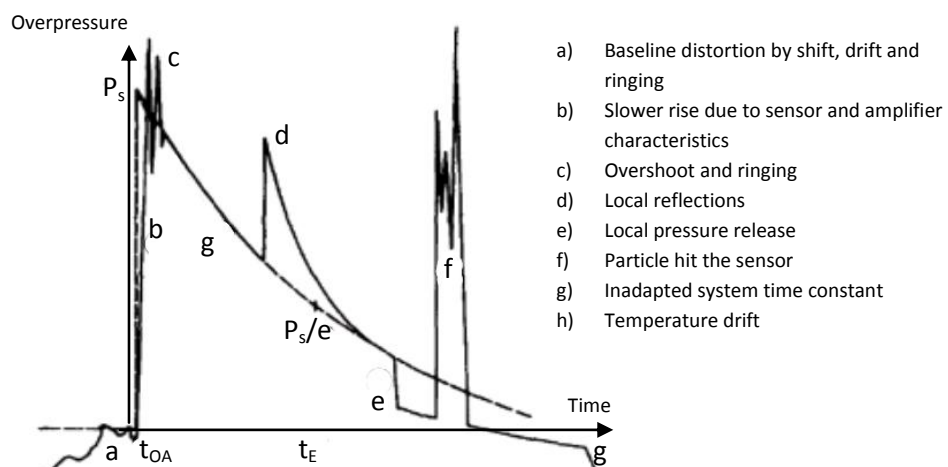


Figure 6.7: Some features observed on pressure records (dashed line: “true signal”, full: sensor record).

6.4 Impulse calculation from pressure record

The positive impulse is usually estimated by the integral trapeze method applied to the pressure record. However, some pressure signals present particularities described in figure 6.7, like overshoots thermal drift in the release or Mach reflection (fig. 6.8) that gives over estimations on the positive impulse with the application of the trapeze method. The estimation of the positive impulse depends thus on the method adopted. One of the possibilities is to consider the best Friedlander fit given by expression (3.1), from the region between the overshoot and the perturbation (reflexion, ...). The impulse is then calculated from the fit (fig. 6.8 left). It can also be calculated from a flat fee method that consists of considering the positive peak until the release reaches 10 % of the peak pressure P_{max} (fig 6.8 right). It has been observed that both methods are in agreement within 10 % discrepancy with CONWEP and UFC-3-340-2 data [Bailleau, 2013].

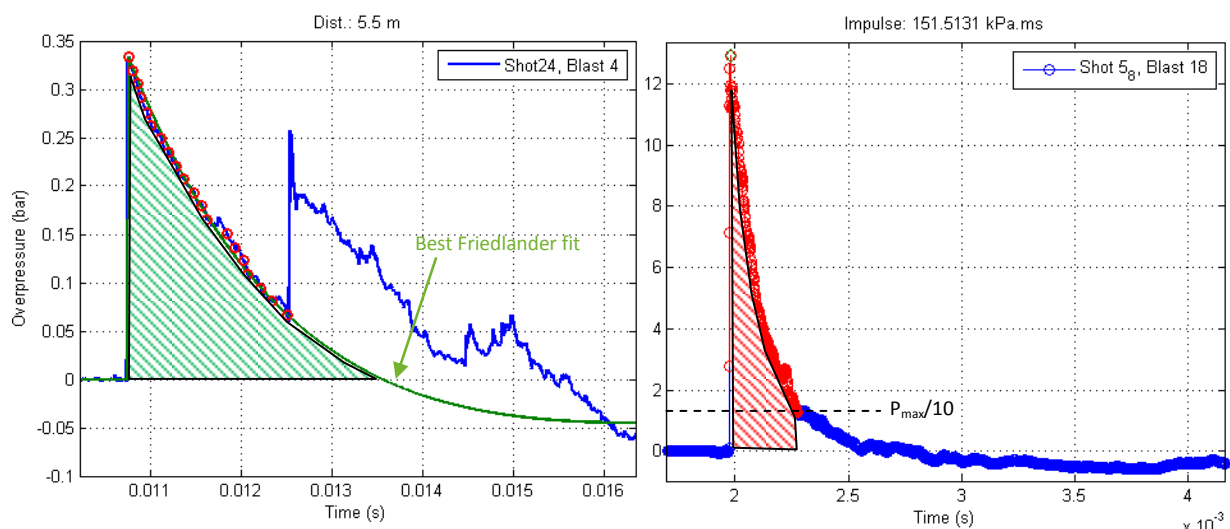


Figure 6.8: Different methods for the positive impulse calculation. (left) by Friedlander fit method, (right) by the flat fee method).

7. Planar oblique shock waves

Shockwaves can be broadly divided in three categories:

- Normal (planar) shockwaves,
- Oblique planar shockwaves (with respect to the flow, cf. fig. 7.2),
- Non-planar shockwaves.

Non-planar shockwaves are obviously the more complex to study, and no general analytical model can be established to determine the mechanical and thermodynamical states of the shocked medium in this case. Excluding some very particular cases, blast waves are non-planar. No matter the shape of an explosive charge, the curvature of the blast wave it generates decreases as the wave travels away from the point of explosion, to the point where it can be assumed quasi-planar. In this respect, models valid for planar shockwaves, and in particular oblique waves, can be used to study blast waves.

It can be shown that shockwaves are a consequence of the hyperbolicity of the system of Euler equations governing inviscid flows. From a more factual point of view, normal and oblique planar

shockwaves can be observed in many supersonic flows, and most notably in propulsive systems (air inlets, nozzles, scramjets, etc.). The appearance of such a discontinuity is inevitably linked to one of two phenomena:

- The need to match pressures in different areas of a supersonic flow. If the wave is oblique, this will induce a deflection of the flow.
- The need to deflect the flow (because of an obstacle, for instance). The presence of an obstacle in a subsonic flow induces acoustic perturbations which can propagate upstream. This establishes a pressure gradient in front of the obstacle, leading to a decrease in flow velocity, a deflection of the streamlines, and eventually to a stagnation point. In the case of a supersonic flow, acoustic perturbations cannot propagate upstream. Fluid particles therefore cannot be “warned” of the presence of an obstacle and adjust their velocity consequently. In this case, an oblique planar shockwave (or a curved shockwave) appears in front of the obstacle to allow the deflection of the flow.

The mechanical and thermodynamical states of the shocked fluid can be obtained thanks to compatibility relations based on the conservation of mass, momentum and energy. These relations are commonly established assuming an inviscid and thermally non-conducting fluid. It is yet worth mentioning that, although its effects can be neglected in many instances, viscosity plays a major part in the physics of shockwaves. In particular, it can be shown that the thickness of the shockwave actually depends on the fluid viscosity, and that viscosity is responsible for the jump in entropy across a shockwave. All shockwaves share common features:

- They require that the flow through them be supersonic with respect to them. This implies that a shockwave propagates at a supersonic velocity in a fluid at rest.
- Unless the medium is in a peculiar thermodynamical state, a shockwave always induces an increase in pressure and a drop in fluid velocity (with respect to the discontinuity). In other words, in normal conditions, rarefaction shockwaves do not exist.
- They are non-isentropic phenomena.

7.1 Conservation laws for a discontinuity (Rankine-Hugoniot relations)

We consider a control volume (D) delimited by surface (S). We denote \vec{n} the outward normal to (S), ρ , \vec{V} , p and u respectively the fluid density, velocity, pressure and internal specific energy. The integral conservation laws for mass, momentum and specific total energy $e_t = u + \frac{1}{2}V^2$ are given by equations (7.1).

$$\begin{aligned} \frac{D}{Dt} \iiint_D \rho dv &= 0 \\ \frac{D}{Dt} \iiint_D \rho \vec{V} dv &= - \iint_S p \vec{n} ds \\ \frac{D}{Dt} \iiint_D \rho \left(u + \frac{1}{2} V^2 \right) dv &= - \iint_S p \vec{V} \cdot \vec{n} ds \end{aligned} \quad (7.1)$$

If we consider the case of a control volume split by a discontinuity (Σ) moving at an arbitrary celerity \vec{D} , as illustrated in figure 7.1, two subdomains respectively denoted (Δ_1) and (Δ_2) can be distinguished. Unlike domain (D), these are not material domains, since one of their boundaries (Σ) has a velocity not equal to the fluid velocity. One can show that integrating equations (7.1) for such a domain yields relations (7.2).

$$\begin{aligned}
 \{\rho \vec{W} \cdot \vec{N}\} &= 0 \\
 \{[\rho \vec{V} \cdot \vec{W} + p] \vec{N}\} &= 0 \\
 \left\{ \left[\rho \left(u + \frac{1}{2} V^2 \right) \vec{W} + p \vec{V} \right] \cdot \vec{N} \right\} &= 0
 \end{aligned} \tag{7.2}$$

\vec{N} stands for the normal to the discontinuity, arbitrarily oriented from domain (Δ_1) to (Δ_2), and $\vec{W} = \vec{V} - \vec{D}$ for the fluid velocity relative to the discontinuity. The operator $\{ \}$ stands for the difference of the quantity in braces evaluated on both sides of the discontinuity.

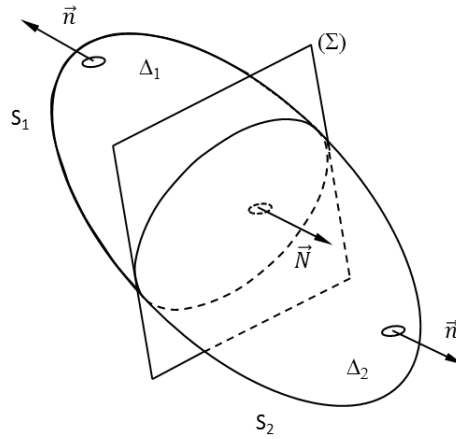


Figure 7.1: control volume split by a surface of discontinuity

In the case of a normal steady ($\vec{D} = Cte$) shockwave, relations (7.2) simplify to relations (7.3). The subscripts $_1$ and $_2$ refer to either side of the discontinuity, and h stands for the specific enthalpy.

$$\begin{aligned}
 \rho_1 \vec{W}_1 &= \rho_2 \vec{W}_2 \\
 p_1 + \rho_1 \vec{W}_1^2 &= p_2 + \rho_2 \vec{W}_2^2 \\
 h_1 + \frac{1}{2} \vec{W}_1^2 &= h_2 + \frac{1}{2} \vec{W}_2^2
 \end{aligned} \tag{7.3}$$

Denoting c the sound velocity, $M_1 = \frac{|W_1|}{c_1}$ stands for the algebraic Mach number of the wave with respect to the unshocked fluid. If the fluid is assumed to be initially at rest, M_1 is therefore the Mach number of the wave in the laboratory frame. Assuming the fluid is a calorically perfect gas (i.e. γ is a constant) and introducing the corresponding equation of state ($p = \rho RT$), relations (7.3) can easily be transformed to obtain the well-known Rankine-Hugoniot relations for a planar normal steady shockwave (7.4).

$$\begin{aligned}
 \sigma &= \frac{\rho_1}{\rho_2} = \frac{(\gamma-1)M_1^2+2}{(\gamma+1)M_1^2} \\
 \varpi &= \frac{p_2}{p_1} = \frac{2\gamma M_1^2-\gamma+1}{\gamma+1} \\
 V_2 - V_1 &= -\frac{2W_1}{\gamma+1} \left(1 - \frac{1}{M_1^2} \right)
 \end{aligned} \tag{7.4}$$

$$M_2^2 = \frac{(\gamma-1)(M_1^2-1)+\gamma+1}{2\gamma(M_1^2-1)+\gamma+1}$$

Relations (7.4) show that the knowledge of Mach number M_1 is required to determine the state of the shocked fluid. This Mach number depends on the phenomena which generated the shockwave (moving piston, explosive charge, tank breach, etc.). These relations furthermore show that $M_2 < 1$: the wave is subsonic with respect to the shocked fluid, meaning that following acoustic waves can catch up and interfere with the head shockwave, dampening or strengthening it.

7.2 Oblique planar shockwaves

In the following, we assume that $\vec{D} = \vec{0}$ (i.e. $\vec{W} = \vec{V}$), which amounts to working in a frame linked to the steady shockwave. Figure 7.2 shows the structure of an oblique planar wave. As stated previously, the pressure jump across the wave is associated with a deflection of the streamlines. In addition to the incident Mach number M_1 , two other parameters are needed to characterize the wave:

- The angle of deflection δ ,
- The shock angle θ .

Both angles are measured taking the initial flow direction as a reference.

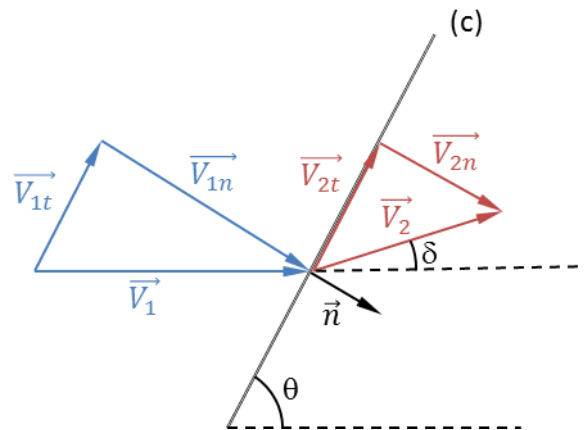


Figure 7.2 : planar oblique shockwave

In order to determine state 2, it is convenient to work with a frame attached to the wave. Introducing subscripts n and t, velocities are decomposed in their normal and tangential components with respect to the wave.

$$\begin{aligned} V_{1n} &= V_1 \sin \theta & V_{2n} &= V_2 \sin(\theta - \delta) \\ V_{1t} &= V_1 \cos \theta & V_{2t} &= V_2 \cos(\theta - \delta) \end{aligned}$$

Equations (7.2) then readily yield relations (7.5).

$$\begin{aligned} \rho_1 V_{1n} &= \rho_2 V_{2n} \\ p_1 + \rho_1 V_{1n}^2 &= p_2 + \rho_2 V_{2n}^2 \\ V_{1t} &= V_{2t} \end{aligned} \quad (7.5)$$

$$h_1 + \frac{1}{2}V_{1n}^2 = h_2 + \frac{1}{2}V_{2n}^2$$

Relations (7.5) show that the tangential velocity is conserved through the shockwave and that the properties of state 2 can be determined using the Rankine-Hugoniot relations (7.4), provided the normal Mach number is used ($M_{1n} = \frac{V_{1n}}{c_1}$). This requires the prior determination of the shock angle θ . Writing the conservation of mass flow through the shock, one can obtain the implicit equation (7.6), which can be solved to obtain θ .

$$\frac{\tan(\theta-\delta)}{\tan\theta} = \frac{\gamma-1}{\gamma+1} \left(1 + \frac{2}{(\gamma-1)M_1^2 \sin^2\theta} \right) \quad (7.6)$$

Using basic trigonometric relations, equation (6) can be rewritten as relation (6'), which can be more convenient to handle.

$$\frac{1}{\tan\delta} = \left(\frac{\gamma+1}{2} \frac{M_1^2}{M_1^2 \sin^2\theta - 1} - 1 \right) \tan\theta \quad (7.6')$$

Equation (7.6) usually has several solutions, among which only two have physical meaning.

Plotting θ as a function of δ for a given Mach number M_1 gives the shock polar in the (δ, θ) plane (figure 7.3). Several features of figure 7.3 require further comments:

- The shock polar shows that for a given incident Mach number, a maximum deflection exists, above which the current solution is no longer possible. The value of the maximal deflection tends towards 45.585° (for $\gamma = 1.4$) for an infinite incident Mach number. Should the flow require a deflection larger than this maximum value (in the case of a blunt obstacle, for instance), its structure will drastically change, and a detached shockwave will appear.
- The dotted line marks the separation between weak and strong shocks, corresponding to the aforementioned valid solutions to equation (7.6). The weak shock is the thermodynamically preferential solution and will therefore appear in a spontaneous evolution. In other words, a strong shock will most often appear only if it is somewhat forced (the most notable exception being the Mach stem, as will be seen in §7.3). Understandably, the pressure jump is larger across the strong shockwave.
- The Rankine-Hugoniot relations ensure that the normal Mach M_{2n} is smaller than 1 (cf. §7.1). Since the wave Mach number with respect to the shocked fluid M_2 is given by $M_2 = \frac{M_{2n}}{\sin(\theta-\delta)}$, it is possible for this number to be greater than unity. This depends on the values on M_1 and δ , as illustrated by the black full line on figure 7.3. Solutions located above this line have a subsonic value for M_2 .

To sum it up, to determine the state of the shocked fluid behind an oblique planar shock wave knowing the incident Mach number M_1 and the deflection angle δ , the following steps should be followed:

1 – Calculate the shock angle θ using relation (7.6). This requires a numerical solver. In case of doubt, use the shock polar (fig. 7.3) to choose the angle value corresponding to the weak shock (unless you know you are dealing with a strong shock). Alternatively, the shock polar can be used to determine the shock angle graphically, although this yields less accurate results.

2 – Calculate the normal incident Mach number M_{1n}

3 – Use the Rankine Hugoniot relations (7.4) to calculate the pressure, density, velocity and normal Mach number M_{2n} . The temperature can be obtained with the ideal gas equation of state, if needed.

4 – Calculate the shocked fluid Mach number with respect to the shockwave M_2 .

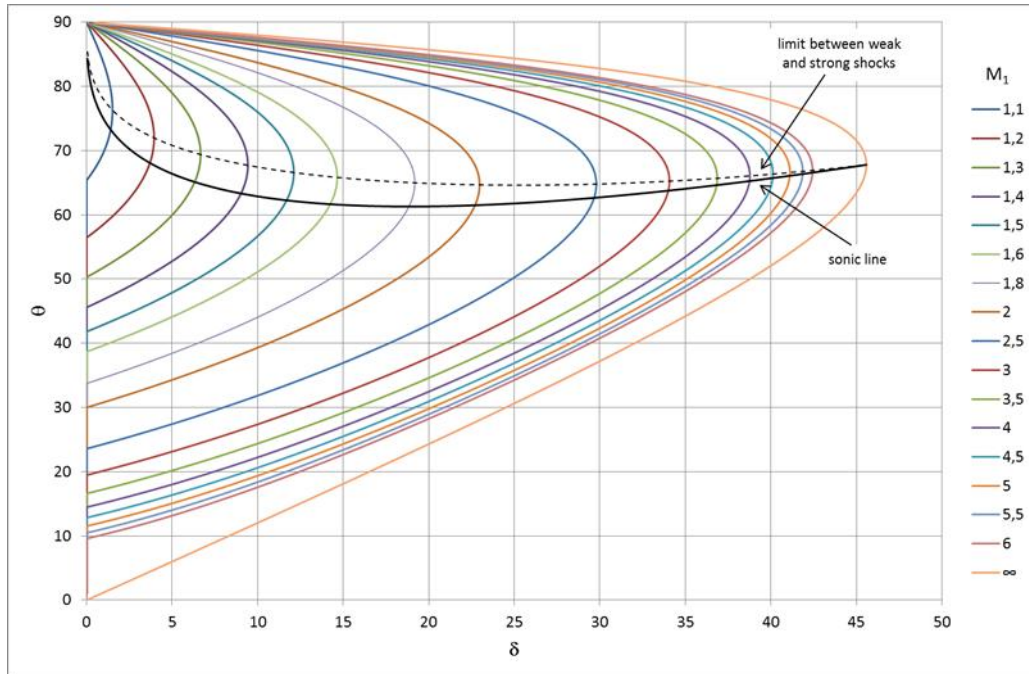


Figure 7.3 : shock polars in the (δ, θ) plane for several Mach numbers ($\gamma = 1.4$)

The shock polar can also be plotted in the (δ, p) plane (figure 7.4), recovering all the features of the (δ, θ) shock polar. We will see in §7.3 that this polar is more useful than the first one to study shockwave interactions. Depending on deflection δ , several cases can be considered:

- $\delta = 0$. Two solutions exist, respectively corresponding to an evanescent shock ($M_1 = 1 + \varepsilon$) and a normal shockwave.
- $\delta < \delta_{max}$. Three solutions are obtained, corresponding to a rarefaction shock (which, as a reminder, is a non-physical solution for most cases and should be discarded), a weak shock (lower branch) and a strong shock (upper branch).
- $\delta = \delta_{max}$. Only one solution is obtained.

Plotting this polar is quite straightforward if you use the shock angle as a parameter in relations (7.4) and (7.6'):

$$\frac{1}{\tan \delta} = \left(\frac{\gamma + 1}{2} \frac{M_1^2}{M_1^2 \sin^2 \theta - 1} - 1 \right) \tan \theta$$

$$\frac{p}{p_1} = \frac{2\gamma M_1^2 \sin^2 \theta - \gamma + 1}{\gamma + 1}$$

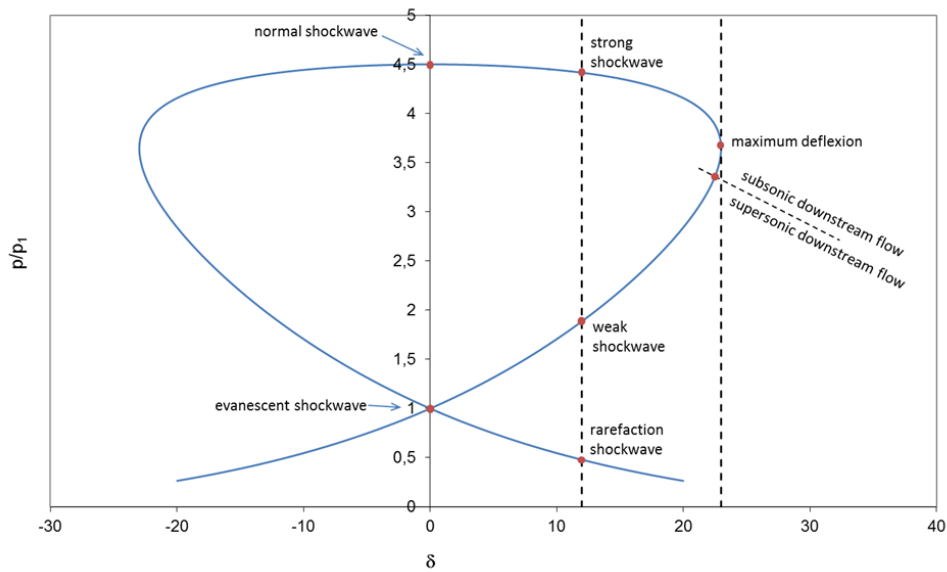


Figure 7.4 : shock polar in the (δ, p) plane

Figure 5 shows the evolution of the (δ, p) shock polar when the incident Mach number is increased. The asymptotic value for the maximum deflection (45.585° for $\gamma = 1.4$) is also apparent on this plot. Incidentally, it is worth noting that for high Mach numbers, the calorically perfect gas assumption may prove insufficient. Indeed, high temperature dissociation will lead to non-negligible variations of γ . As an example, with $\gamma = 1.4$, the calorically perfect gas model predicts that the temperature is multiplied approximately by 20 for $M_1 = 10$, yielding temperatures way over 2000K, which is commonly accepted as the limit from which molecular dissociation should be taken into account.

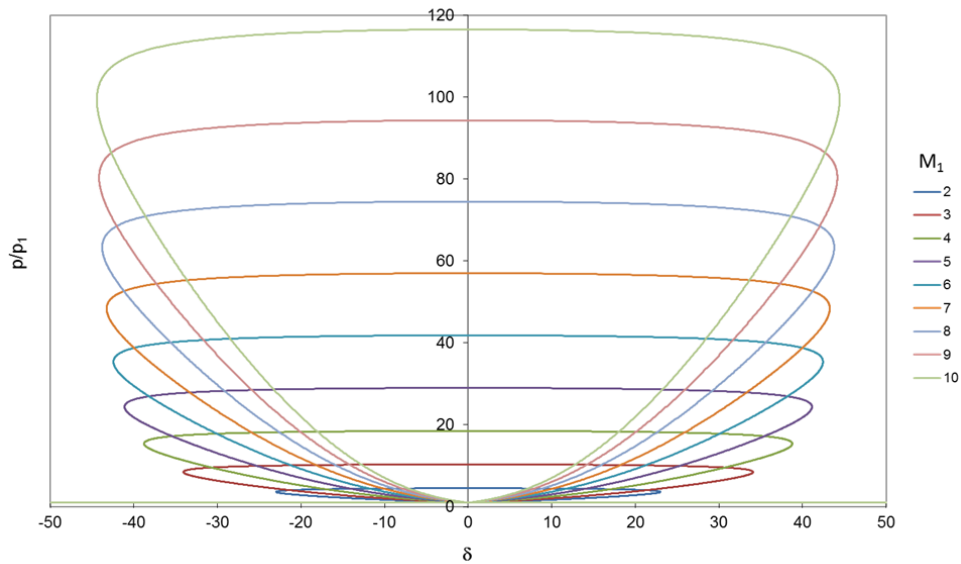


Figure 7.5 : shock polars in the (δ, p) plane for several Mach numbers ($\gamma = 1.4$)

7.3 Shockwave reflection

We first consider the case of a normal wave progressing toward a fixed wall, in a gas initially at rest, as illustrated in figure 6a. In state (2), the fluid velocity V_2 is non-zero, which is incompatible with the boundary condition on the wall ($V = 0$). A reflected shockwave is generated, in order to bring the fluid velocity to zero ($V_3 = 0$). State (3) can be determined using the conservation laws for a steady normal discontinuity (3), noticing that $V_1 = V_3 = 0$. Given the pressure ratio ϖ_i across the incident shockwave, the pressure ratio across the reflected shockwave ϖ_r is given by relation (7.3).

$$\varpi_r = \frac{(3\gamma-1)\varpi_i - (\gamma-1)}{(\gamma-1)\varpi_i + (\gamma+1)} \quad (7.3)$$

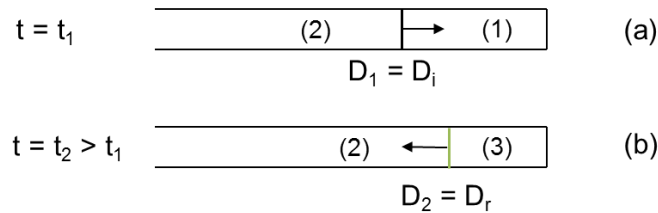


Figure 7.6 : reflection of a normal shockwave on a wall

The case of an oblique shockwave impinging on a wall is illustrated in figure 7.7, in the case of a uniform flow in a channel. The incident wave S_1 (blue line) is created by a sudden change in the channel cross-section, inducing a deflection with angle δ . The red line depicts the trajectory of a fluid particle. Upon reaching the upper wall, the deflected fluid must be deflected again, so that the flow direction is parallel to the wall. A second shockwave S_2 is therefore created (green line). Knowing the Mach number of the flow and the angle of the incident shock, states 2 and 3 can easily be successively determined using the method highlighted in §2.7.

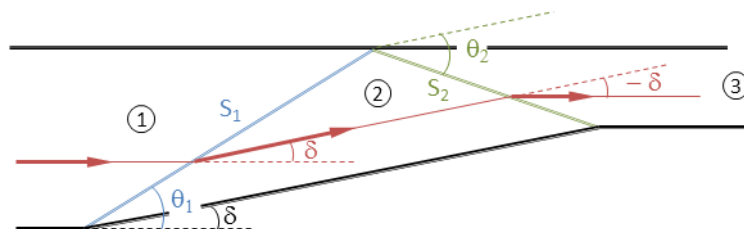


Figure 7.7 : regular reflexion
Blue: incident shock, green: reflected shock, red: particle trajectory

Alternatively, the problem can be solved using the (δ, p) shock polar, as shown in figure 7.8. In this picture, we have kept the colours associated to each wave in picture 7.7. Plotting the polar of the incident shockwave is actually not mandatory: locating point 2 is sufficient. From there, the polar of the reflected shock is plotted, using state 2 as the pole. We know that in state 3 the flow must have recovered its initial direction (i.e. $\delta = 0$). The point representing state 3 therefore lies at the intersection between the reflected shock polar and the vertical axis. When deflection δ is increased, point 2 moves along the incident shock polar and the reflected shock polar must be plotted for each case, as shown in figure 7.9. If the deflection becomes too large, a situation is reached where the reflected shock polar no longer intersects the vertical axis and the flow structure depicted in figure 7.7 is no longer valid. The polar in red in figure 7.9 has a vertical tangent with the y-axis and corresponds to the limit case of the regular reflection.

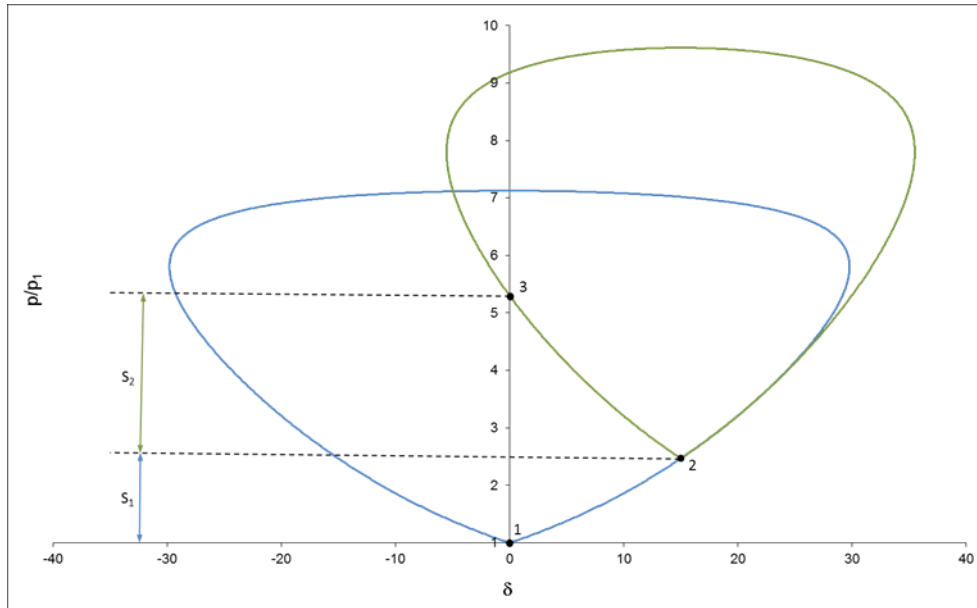


Figure 7.8: (δ, p) shock polars for a regular reflexion
Blue: incident shock, green: reflected shock

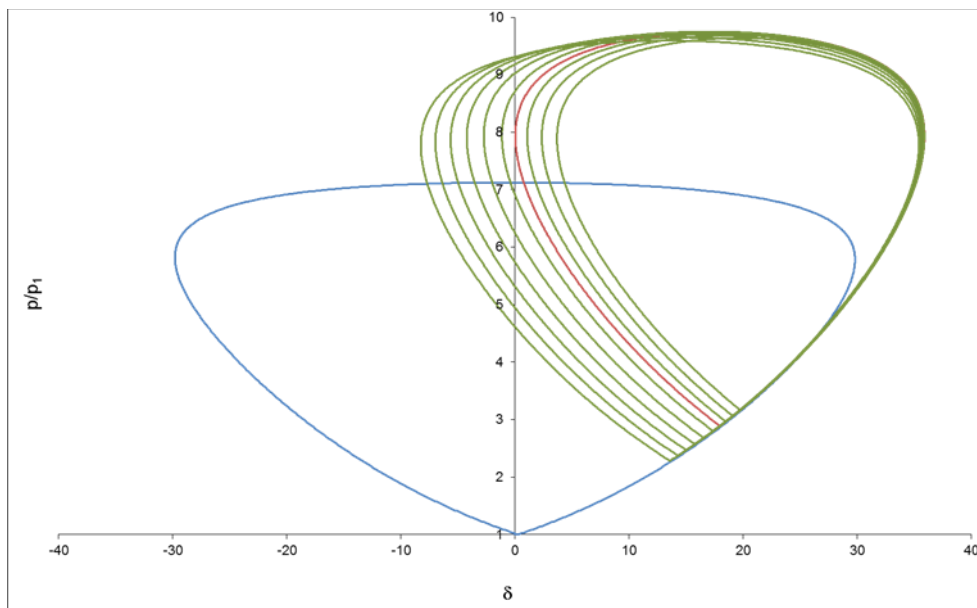


Figure 7.9: transition from a regular to a singular reflexion
Blue: incident shock, green: reflected shock

When the regular reflection is not possible, the flow structure becomes more complex, as illustrated in figure 7.10 for a uniform flow in a channel. In this case, referred to as a singular reflection, a third shockwave S_3 appears, between the incident and reflected waves and the upper wall. All three waves intersect at point T, called a triple point. Two trajectories are thus possible for fluid particles, depending on whether they go through the incident and reflected shockwaves, or through the Mach stem, and leading respectively to states 3 and 4. Right behind the reflected wave and the Mach stem, states 3 and 4 must be at the same pressure, otherwise an additional wave (a shock or a rarefaction wave) would be required between them. These states are separated by what is called a surface of

contact, denoted D on figure 7.10. This is basically a discontinuity across which no mass flow rate exists (unlike shockwaves), which implies that all variables but the pressure may vary through the discontinuity. This can be readily shown by solving equations (7.2) with the assumption of a nil mass flow rate across the discontinuity. Foregoing the inviscid assumption, a mixing layer due to the diffusion of momentum would be observed instead. Unlike the case of the regular reflection, states 3 and 4 are not uniform. This is due to the fact that the Mach stem is not a planar wave, but instead a quasi-planar wave, and deflects the flow. Two stream tubes, bounded by the contact surface appear. Conservation of mass and momentum in either tube leads to different fluid accelerations, whether the stream tubes expand or constrict.

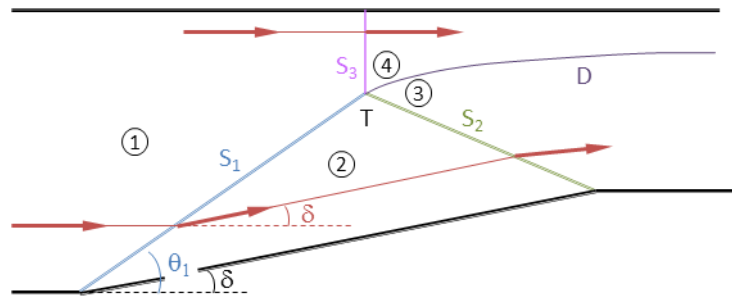


Figure 7.10: singular reflexion
Blue: incident shock, green: reflected shock, purple: Mach stem, red: particle trajectory

The case of the singular reflection can be solved using the (δ, p) shock polars. As in the previous case, the polars corresponding to the incident and reflected waves (i.e. for poles corresponding to states 1 and 2) are plotted. State 3 must be on the polar associated with the reflected wave, while state 4 must lie on the polar associated with the incident wave (since the fluid is in state 1 before the Mach stem). Right behind the waves, states 3 and 4 have the same pressure and flow direction and thus are represented by the same point in the (δ, p) plane, which is the intersection between both polars. The Mach stem is therefore a strong shock, and is most often almost normal.

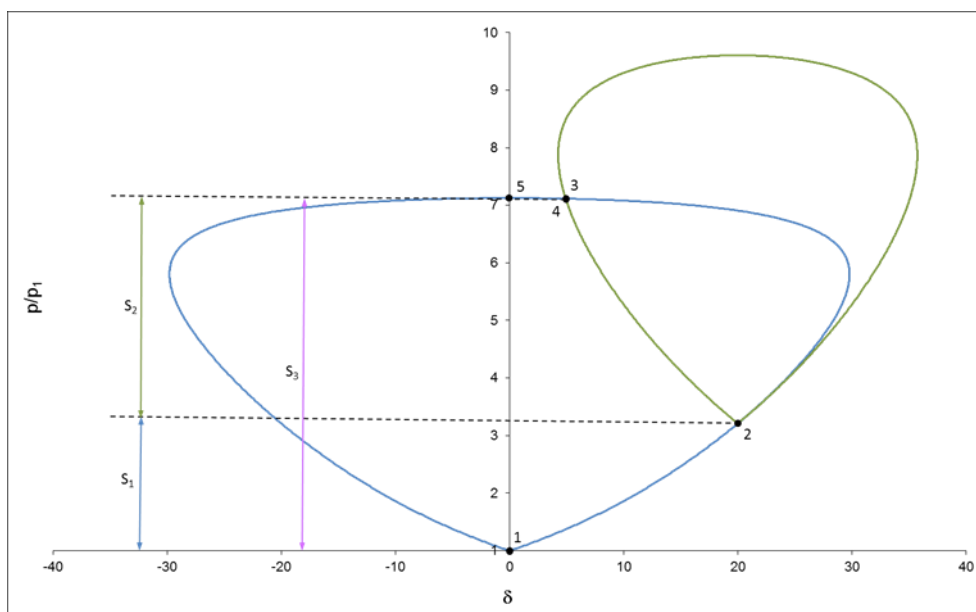


Figure 7.11: shock polars for a singular reflexion
Blue: incident shock, green: reflected

8. Blast mitigation

8.1 Aqueous foams

Peregino et al. experimented, in 1998, blast and fragment suppression by aqueous foam and a Kevlar® tent. The tent was set on a bare cylindrical explosive charge of composition B (40% TNT, 60% RDX). Various charge weight were experimented: 113.5 g, 227.0 g, and 340.5 g. The L/D (length/diameter) of all the charges was 1. They measured overpressure with pencil blast located at 1.5 m, 4 m and 7.6 m. They could observe that for a given distance, whatever the charge weight, the ratio of the peak of overpressure measured with and without foam is almost conserved and increased with the distance. They obtained around 1.5 %, 3.5 % and 5 % of residual overpressure at respectively 1.5, 4 and 7.6 m.

These promising preliminary results attracted the interest of the scientific community. Hartman et al. 2006, presented a series of experiments on blast mitigation capabilities of aqueous foams with several expansion ratio, ranging from 10:1 to 1000:1. They concluded that aqueous foams are efficient in mitigating the blast resulting from a high explosive detonation. They could propose empirical relations for describing the overpressure (fig. 8.1) and time of arrival versus scaled distance for several expansion ratios. They obtained a better mitigation with 60:1 expansion ratio. They explained that an important part of the pressure loss brought by the aqueous foam is due to the impedance mismatch between air and the biphasic medium but also by internal reflections at the numerous air-liquid interfaces within the foam. They also highlight the fact that the breakup of the foam and the vaporizing of the liquid phase play an important role in the energy dissipation.

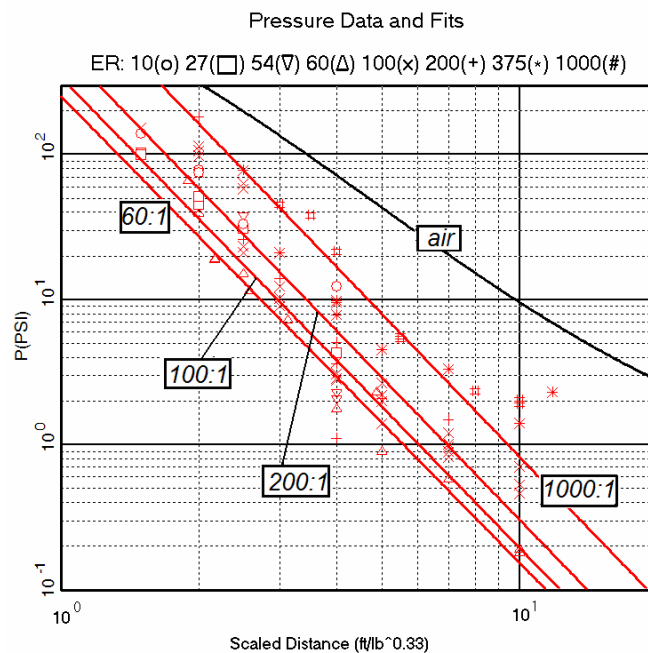


Figure 8.1: Evolution of the blast pressure versus scaled distance for various foam expansion ratios. [Hartman 2006]

8.2 Blast mitigation by water mist/droplet clouds

Initially, spherical water droplets were used for fires extinction. This technique has been studied since more than 60 years. In this purpose, atomisation techniques allow obtaining water mists with calibrated droplet sizes that can be typically from 1 μm up to 2.5 mm. Borisov et al carried out a work

on shock mitigation by water mist [Borisov, 1971]. Since the early twenty one century, the scientific community has manifested an increasing interest on using water mist as a solution for blast mitigation. One of the physical identified phenomenons yielding to blast mitigation is the secondary atomisation: when an initially spherical droplet is stricken by a blast wave, it undergoes hydrodynamic forces that distort it. Hydrodynamic instabilities also participate in such a distortion. At last, when these distortions are too important regarding the flow parameters (bubble size and mach of the flow), droplets split into a cloud of smaller droplets that are even easier to vaporise and thus, they absorb even more energy to the shock front.

Recently Chauvin et al. [Chauvin, 2011] carried out shock tube experiments in order to observe shock propagation through calibrated clouds of 1.2% of volume fraction of droplets of about $D_d=500 \mu\text{m}$ diameter. Clouds were trapped at the extremity of the shock tube. Several length of clouds, H_d , were studied, 150 mm, 400 mm, and 700 mm. Authors used two Mach numbers, 1.3 and 1.5. They could evidence that in some situation, the overpressure was diminished of about 80%. Figure 8.2 gathers their experimental results. They observed a loss of pressure when the reduced parameter \uparrow increases, with:

$$\uparrow = \frac{S_e W_e}{a^2 \sqrt{Re}} \quad (8.1)$$

Where S_e is the specific surface of droplets crossed by the shock wave:

$$S_e = n\pi D_d^2 \quad (8.2)$$

with n the number of droplets crossed by the shock wave:

$$n = N_d \cdot h_d / H_d \quad (8.3)$$

Where h_d is the distance travelled by the shock into the cloud and N_d the total number of droplets in the cloud (8.4) :

$$N_d = \frac{6 V_w}{\pi D_d^3} \quad (8.4)$$

The Reynolds and Weber numbers respectively noted Re and We , are expressed as follow (8.5) and (8.6):

$$Re = \frac{\rho^* u D_d}{\mu} \quad (8.5)$$

$$We = \frac{\rho^* u^2 D_d}{\sigma} \quad (8.6)$$

With ρ^* the gas density for a given Mach number, u the particular velocity, μ the gas viscosity and σ the surface tension. Table 8 gives the values of shock parameters.

Ma	u (m/s)	ΔP (bar)	ρ^* (kg/m ³)	Re	We
1.3	152	0.81	1.8	8200	331
1.5	238	1.46	2.2	14000	824

Table 8 : Shock parameters in the flow.

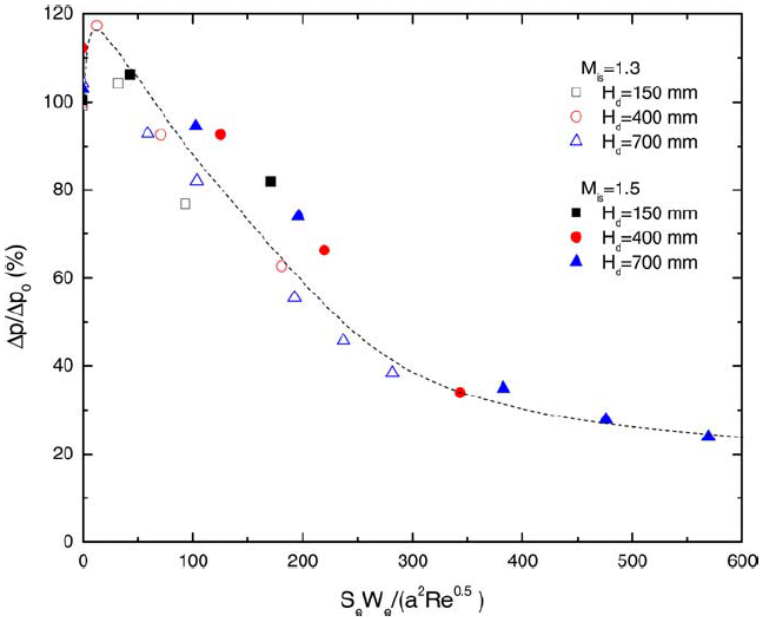


Figure 8.2: Overpressure mitigation by water mist in shock tube experiments, for two Mach numbers, 1.3 and 1.5, for three different mist length, $H_d=150, 400$ and 700 mm [Chauvin, 2011].

References :

- Bach, G. G., and J. H. S. Lee. "An analytical solution for blast waves." *AIAA journal* 8.2 (1970): 271-275.
- Bailleau G., Influence de la forme d'une charge d'explosif cylindrique sur le champ de pression, MSc University of Poitiers, 2013 (in french).
- Baker, Wilfred Edmund, et al. *Explosion hazards and evaluation*. Elsevier, 2012.
- Borisov A. A., Gel'fand B. E., Gubin S. A., Kogarko S. M., and Krivenko S. M., "Attenuation of shock waves in a two-phase gas-liquid medium," *Mekhanika Zhidkosti i Gaza* 5, 176 (1971).
- Bowen I., Ray J., "Dynamics of exothermicity : In honour of A. K. Oppenheim", ISBN 2-88449-5519, vol 2, Gordon and Breach publishers, 1996.
- Brode, Harold L. "Blast wave from a spherical charge." *Physics of Fluids (1958-1988)* 2.2 (1959): 217-229.
- Chauvin A., Jourdan G., Daniel E., Houas L., and Tosello R., "Experimental investigation of the propagation of a planar shock wave through a two-phase gas-liquid medium", *PHYSICS OF FLUIDS* 23, 113301 (2011), doi:10.1063/1.3657083.
- Cole, Robert Hugh. "Underwater Explosions.", Princeton university press, 1948.
- Cooper, Paul W., Stanley R. Kurowski, and Paul W. Cooper. *Introduction to the Technology of Explosives*. New York: VCH, 1996.
- Dobratz, B. M., and P. C. Crawford. "LLNL Handbook of Explosives, UCRL-52997, Lawrence Livermore National Laboratory." *Change* 2 (1985): 8-21.
- Esparza, E. D., *Spherical equivalency of cylindrical charges in free-air*, 25th Department of Defense Explosives Safety Seminar, Aug. 1982,
- Gross K. "Phenomenological Model for Infrared Emissions from High-Explosive Detonation Fireballs », dissertation of the air force air university, 2007.
- Guerke G., "Evaluation of blast pressure measurements", Fraunhofer-Institut für Kurzezeitdynamik, Ernst-Mach-Institut -EMI-, Freiburg/Brsg, 1990.
- Hardesty, D. R., and J. E. Kennedy. "Thermochemical estimation of explosive energy output." *Combustion and Flame* 28 (1977): 45-59.
- Hartman W. F., Boughton B. A., Larsen M.E. "Blast Mitigation Capabilities of Aqueous Foam", SANDIA REPORT, SAND2006-0533, 2006.
- Henrych, Josef, and Rudolf Major. *The dynamics of explosion and its use*. Amsterdam: Elsevier, 1979.
- Ismail M. and Murray S., 1993, *Study of the Blast Waves from the Explosion of Nonspherical Charges*, Propellants, Explos. and Pyrotech., 18, 132–138.
- Kamlet, Mortimer J. and Jacobs, S. J., " Chemistry of Detonations. I. A Simple Method for Calculating Detonation Properties of C–H–N–O Explosives", *The Journal of Chemical Physics*, 48, 23-35 (1968), DOI:<http://dx.doi.org/10.1063/1.1667908>
- Katselis, G., Anderson, J.G., *Estimation of Blast Overpressure From a Cylindrical Charge Using Time of Arrival Sensors*, 14th Australasian Fluid Mechanics Conference, Adelaide University, Adelaide, Dec. 2001
- Keshavarz, Mohammad Hossein, and Mohsen Oftadeh. "A new correlation for predicting the Chapman-Jouguet detonation pressure of CHNO explosives." *HIGH TEMPERATURES HIGH PRESSURES* 34.4 (2002): 495-498.
- Kingery, Charles N. *Air blast parameters versus distance for hemispherical TNT surface bursts*. No. BRL-1344. ARMY BALLISTIC RESEARCH LAB ABERDEEN PROVING GROUND MD, 1966.
- Kinney, Gilbert Ford, and Kenneth Judson Graham. "Explosive shocks in air." *Berlin and New York, Springer-Verlag*, (1985).

Krehl Peter O. K., "History of Shock Waves, Explosions and Impact: A Chronological and Biographical Reference", Springer Science & Business Media, 24 sept. 2008

Lefrançois, A., Delcor, P., *Blast Effects of Cylindrical Bare Charges*, 17th International Symposium on Military Aspects of Blast and Shock, June 2002.

Locking P. "The Trouble with TNT equivalence", 26th ISB, Miami, 2011.

Maximilian Lackner (éd.), Franz Winter (éd.), Avinash K. Agarwal (éd.), *Handbook of Combustion*, John Wiley & Sons, juin 2010 (ISBN 978-3-527-32449-1)

Meyer R., Köhler J., Homburg A., *Explosives*, 6th Edition, Wiley, ISBN: 978-3-527-31656-4, July 2007.

Péchoux, F. "Etude en champs proche de différent types de charges", MSc thesis ENSIETA, 2010 (in french).

Peregino, P. J., Bowman, D., Maulbetsch, R., Saunders, D., & Kieft, L. V. "Blast and fragmentation suppression with aqueous foam and a Kevlar tent." 28th Dep. Def. Exp. Saf. Sem., Orlando, FL. (1998).

Plooster, M. N., *Shock waves from Line Sources*, National center for Atmospheric Research, Boulder, Colorado, Nov. 1968

Plooster, M.N., *Blast Effects from Cylindrical Explosive Charges: Experimental Measurements*, Naval Weapons Center Report No.NWC TP 6382, Chia Lake, CA, 1982

Sakurai, Akira. "On the propagation and structure of the blast wave, I." *Journal of the Physical Society of Japan* 8.5 (1953): 662-669.

Simoens B., Lefebvre M.H., Minami F., "Influence of different parameters on the TNT-equivalent of an explosion", 2011

Simoens B., Lefebvre M.H., Arrigoni M., Kerampran S., "Effect of charge shape: Pressure field around a cylindrical explosive charge", Conference Military Aspects of Blast and Shock, Bourges, France, november 2012.

Taylor, Geoffrey. "The formation of a blast wave by a very intense explosion. I. Theoretical discussion." *Proceedings of the Royal Society of London. Series A, Mathematical and Physical Sciences* (1950): 159-174.

UFC-3-340-2 « Unified Criteria Facilities : Structures to resist the effects of accidental explosions », 2014, http://www.wbdg.org/ccb/DOD/UFC/ufc_3_340_02.pdf

United Nations, "Recommendations on the transport of dangerous goods", ST/SG/AC.10/11/Rev.5, 2009, <http://www.unece.org/fileadmin/DAM/trans/danger/publi/manual/Rev5/English/ST-SG-AC10-11-Rev5-EN.pdf>

Wu, C., Fattori, G., Whittaker, A., Oehlers, D.J., *Investigation of Air-Blast Effects from Spherical- and Cylindrical-Shaped Charges*, Int J. Protective Structure, vol1.3, 2010

ANNEXE A.1: Blast parameters plotted on figure 4.2

Z (m/kg ^{1/3})	Pr (Mpa)	Pso (Mpa)	Ir/W ^{1/3} (Mpa.ms/kg ^{1/3})	Is+/W ^{1/3} (Mpa.ms/kg ^{1/3})	ta/W ^{1/3} (ms/kg ^{1/3})	td/W ^{1/3} (ms/kg ^{1/3})	U(km/s)	Lw(m/kg ^{1/3})
0,0524	629,4854	49,3082	82,8652	2,6590	0,0076	0,2109	6,6514	1,0548
0,0541	612,7594	48,4420	77,0592	2,5254	0,0078	0,2082	6,5926	1,0018
0,0560	597,0200	47,5433	71,6920	2,3935	0,0081	0,2058	6,5308	0,9495
0,0579	582,0536	46,6178	66,7282	2,2640	0,0084	0,2035	6,4666	0,8981
0,0598	567,6828	45,6709	62,1355	2,1377	0,0087	0,2014	6,4004	0,8480
0,0619	553,7651	44,7072	57,8843	2,0150	0,0090	0,1994	6,3326	0,7994
0,0640	540,1872	43,7312	53,9474	1,8965	0,0093	0,1976	6,2635	0,7523
0,0661	526,8569	42,7468	50,3000	1,7825	0,0096	0,1958	6,1934	0,7071
0,0684	513,7031	41,7574	46,9195	1,6733	0,0100	0,1942	6,1226	0,6638
0,0707	500,6720	40,7662	43,7849	1,5690	0,0104	0,1925	6,0513	0,6224
0,0731	487,7270	39,7758	40,8770	1,4698	0,0108	0,1910	5,9794	0,5831
0,0755	474,8401	38,7887	38,1784	1,3757	0,0112	0,1895	5,9072	0,5457
0,0781	461,9972	37,8068	35,6729	1,2867	0,0116	0,1881	5,8348	0,5104
0,0807	449,1895	36,8321	33,3457	1,2028	0,0121	0,1867	5,7621	0,4771
0,0835	436,4183	35,8659	31,1833	1,1238	0,0126	0,1855	5,6893	0,4458
0,0863	423,6899	34,9096	29,1731	1,0496	0,0131	0,1843	5,6163	0,4164
0,0892	411,0132	33,9643	27,3037	0,9801	0,0136	0,1833	5,5432	0,3888
0,0923	398,4027	33,0310	25,5644	0,9151	0,0142	0,1824	5,4699	0,3630
0,0954	385,8735	32,1102	23,9456	0,8544	0,0148	0,1817	5,3965	0,3390
0,0986	373,4430	31,2025	22,4383	0,7979	0,0154	0,1812	5,3230	0,3165
0,1020	361,1289	30,3085	21,0343	0,7452	0,0160	0,1810	5,2493	0,2956
0,1054	348,9500	29,4286	19,7259	0,6962	0,0167	0,1810	5,1754	0,2762
0,1090	336,9228	28,5628	18,5062	0,6507	0,0174	0,1813	5,1014	0,2581
0,1127	325,0659	27,7114	17,3687	0,6085	0,0182	0,1819	5,0273	0,2414
0,1165	313,3944	26,8746	16,3074	0,5694	0,0190	0,1829	4,9531	0,2259
0,1204	301,9222	26,0524	15,3169	0,5331	0,0198	0,1842	4,8787	0,2115
0,1245	290,6638	25,2447	14,3920	0,4996	0,0206	0,1859	4,8042	0,1982
0,1287	279,6308	24,4516	13,5281	0,4686	0,0215	0,1881	4,7296	0,1859
0,1331	268,8322	23,6730	12,7209	0,4399	0,0225	0,1906	4,6550	0,1745
0,1376	258,2777	22,9088	11,9663	0,4134	0,0234	0,1937	4,5803	0,1640
0,1423	247,9735	22,1591	11,2606	0,3889	0,0245	0,1972	4,5057	0,1543
0,1471	237,9258	21,4235	10,6006	0,3663	0,0255	0,2012	4,4310	0,1453
0,1521	228,1373	20,7021	9,9828	0,3455	0,0267	0,2058	4,3564	0,1371
0,1572	218,6115	19,9949	9,4045	0,3263	0,0279	0,2110	4,2820	0,1294
0,1626	209,3504	19,3015	8,8628	0,3086	0,0291	0,2169	4,2076	0,1224
0,1681	200,3541	18,6222	8,3554	0,2922	0,0304	0,2234	4,1335	0,1159
0,1738	191,6219	17,9566	7,8798	0,2772	0,0318	0,2306	4,0595	0,1100
0,1796	183,1517	17,3050	7,4339	0,2633	0,0333	0,2387	3,9857	0,1045
0,1857	174,9428	16,6669	7,0157	0,2506	0,0348	0,2476	3,9123	0,0994

ERASMUS+ “GSEBS” : Arrigoni et al. “Blast waves and propagation and their mitigation”

0,1920	166,9918	16,0426	6,6234	0,2389	0,0364	0,2576	3,8391	0,0948
0,1985	159,2952	15,4319	6,2551	0,2281	0,0381	0,2686	3,7663	0,0905
0,2052	151,8495	14,8349	5,9093	0,2182	0,0398	0,2810	3,6938	0,0865
0,2122	144,6507	14,2515	5,5846	0,2091	0,0417	0,2947	3,6218	0,0829
0,2194	137,6946	13,6817	5,2795	0,2007	0,0437	0,3102	3,5501	0,0796
0,2268	130,9770	13,1255	4,9927	0,1931	0,0458	0,3275	3,4788	0,0766
0,2345	124,4932	12,5829	4,7231	0,1861	0,0480	0,3472	3,4081	0,0738
0,2425	118,2375	12,0540	4,4695	0,1797	0,0503	0,3694	3,3377	0,0713
0,2507	112,2074	11,5388	4,2308	0,1739	0,0527	0,3947	3,2679	0,0690
0,2592	106,3965	11,0371	4,0063	0,1686	0,0553	0,4236	3,1985	0,0669
0,2679	100,8007	10,5493	3,7949	0,1638	0,0580	0,4567	3,1297	0,0650
0,2770	95,4159	10,0750	3,5957	0,1595	0,0609	0,4948	3,0614	0,0633
0,2864	90,2372	9,6144	3,4081	0,1556	0,0640	0,5387	2,9937	0,0617
0,2961	85,2606	9,1675	3,2313	0,1521	0,0672	0,5892	2,9264	0,0603
0,3061	80,4812	8,7342	3,0646	0,1490	0,0707	0,6475	2,8598	0,0591
0,3165	75,8954	8,3146	2,9075	0,1463	0,0743	0,7144	2,7937	0,0581
0,3272	71,4994	7,9086	2,7592	0,1440	0,0781	0,7909	2,7282	0,0571
0,3383	67,2881	7,5160	2,6193	0,1420	0,0822	0,8778	2,6633	0,0563
0,3498	63,2581	7,1370	2,4872	0,1403	0,0865	0,9750	2,5990	0,0557
0,3616	59,4052	6,7714	2,3625	0,1390	0,0911	1,0821	2,5353	0,0551
0,3739	55,7254	6,4190	2,2447	0,1380	0,0960	1,1968	2,4723	0,0547
0,3865	52,2150	6,0798	2,1334	0,1372	0,1012	1,3150	2,4099	0,0544
0,3996	48,8698	5,7536	2,0282	0,1368	0,1067	1,4298	2,3482	0,0543
0,4132	45,6858	5,4402	1,9287	0,1366	0,1126	1,5310	2,2872	0,0542
0,4272	42,6590	5,1396	1,8346	0,1368	0,1188	1,6050	2,2269	0,0543
0,4417	39,7853	4,8515	1,7457	0,1372	0,1254	1,6522	2,1673	0,0544
0,4566	37,0606	4,5757	1,6615	0,1379	0,1325	1,7009	2,1086	0,0547
0,4721	34,4808	4,3119	1,5818	0,1389	0,1400	1,7385	2,0506	0,0551
0,4881	32,0413	4,0600	1,5063	0,1402	0,1480	1,7681	1,9934	0,0556
0,5046	29,7381	3,8197	1,4348	0,1418	0,1565	1,7911	1,9371	0,0562
0,5217	27,5666	3,5907	1,3671	0,1436	0,1655	1,8080	1,8816	0,0570
0,5394	25,5223	3,3727	1,3029	0,1458	0,1752	1,8187	1,8271	0,0578
0,5577	23,6009	3,1655	1,2421	0,1483	0,1855	1,8231	1,7735	0,0588
0,5765	21,7976	2,9687	1,1844	0,1511	0,1965	1,8214	1,7209	0,0600
0,5961	20,1077	2,7820	1,1297	0,1543	0,2082	1,8141	1,6692	0,0612
0,6163	18,5268	2,6052	1,0778	0,1578	0,2207	1,8019	1,6186	0,0626
0,6372	17,0501	2,4378	1,0285	0,1616	0,2340	1,7861	1,5690	0,0641
0,6587	15,6729	2,2796	0,9817	0,1659	0,2482	1,7680	1,5205	0,0658
0,6811	14,3905	2,1301	0,9373	0,1705	0,2633	1,7489	1,4732	0,0676
0,7041	13,1984	1,9892	0,8951	0,1755	0,2795	1,7302	1,4269	0,0696
0,7280	12,0918	1,8564	0,8550	0,1809	0,2967	1,7131	1,3817	0,0718
0,7526	11,0663	1,7313	0,8169	0,1868	0,3151	1,6986	1,3378	0,0741
0,7781	10,1174	1,6138	0,7807	0,1931	0,3348	1,6872	1,2950	0,0766

ERASMUS+ “GSEBS” : Arrigoni et al. “Blast waves and propagation and their mitigation”

0,8045	9,2408	1,5033	0,7463	0,1954	0,3558	1,6795	1,2533	0,0775
0,8318	8,4320	1,3997	0,7135	0,1939	0,3781	1,6756	1,2129	0,0769
0,8599	7,6871	1,3025	0,6824	0,1915	0,4020	1,6755	1,1737	0,0760
0,8891	7,0020	1,2114	0,6527	0,1886	0,4275	1,6790	1,1357	0,0748
0,9192	6,3726	1,1263	0,6245	0,1851	0,4547	1,6859	1,0989	0,0734
0,9503	5,7954	1,0466	0,5977	0,1811	0,4837	1,6963	1,0634	0,0719
0,9825	5,2667	0,9722	0,5721	0,1769	0,5146	1,7100	1,0290	0,0702
1,0158	4,7831	0,9027	0,5477	0,1724	0,5477	1,7276	0,9959	0,0684
1,0502	4,3412	0,8380	0,5245	0,1678	0,5829	1,7496	0,9639	0,0666
1,0858	3,9380	0,7776	0,5023	0,1631	0,6204	1,7770	0,9331	0,0647
1,1226	3,5705	0,7214	0,4812	0,1584	0,6605	1,8113	0,9035	0,0628
1,1606	3,2359	0,6691	0,4611	0,1536	0,7031	1,8539	0,8750	0,0609
1,2000	2,9316	0,6204	0,4419	0,1490	0,7486	1,9059	0,8477	0,0591
1,2406	2,6550	0,5752	0,4236	0,1444	0,7971	1,9679	0,8215	0,0573
1,2826	2,4040	0,5332	0,4062	0,1399	0,8487	2,0384	0,7964	0,0555
1,3261	2,1764	0,4942	0,3895	0,1355	0,9036	2,1126	0,7724	0,0537
1,3710	1,9701	0,4580	0,3736	0,1312	0,9621	2,1847	0,7494	0,0521
1,4175	1,7833	0,4245	0,3584	0,1271	1,0244	2,2513	0,7274	0,0504
1,4655	1,6142	0,3934	0,3439	0,1231	1,0906	2,3145	0,7064	0,0488
1,5151	1,4613	0,3646	0,3300	0,1192	1,1609	2,3742	0,6864	0,0473
1,5665	1,3231	0,3380	0,3167	0,1155	1,2357	2,4308	0,6673	0,0458
1,6195	1,1983	0,3133	0,3041	0,1119	1,3152	2,4845	0,6492	0,0444
1,6744	1,0855	0,2904	0,2920	0,1085	1,3996	2,5354	0,6319	0,0430
1,7311	0,9837	0,2693	0,2804	0,1052	1,4892	2,5839	0,6155	0,0417
1,7898	0,8919	0,2498	0,2693	0,1020	1,5842	2,6301	0,5999	0,0404
1,8504	0,8090	0,2317	0,2587	0,0989	1,6850	2,6743	0,5850	0,0392
1,9131	0,7342	0,2150	0,2486	0,0959	1,7917	2,7167	0,5710	0,0380
1,9779	0,6668	0,1996	0,2389	0,0931	1,9048	2,7576	0,5577	0,0369
2,0449	0,6060	0,1853	0,2296	0,0903	2,0246	2,7971	0,5451	0,0358
2,1142	0,5511	0,1721	0,2207	0,0876	2,1512	2,8354	0,5332	0,0348
2,1858	0,5016	0,1599	0,2122	0,0851	2,2852	2,8727	0,5219	0,0337
2,2599	0,4569	0,1487	0,2041	0,0826	2,4267	2,9091	0,5112	0,0328
2,3364	0,4166	0,1382	0,1962	0,0802	2,5762	2,9449	0,5012	0,0318
2,4156	0,3802	0,1286	0,1888	0,0778	2,7340	2,9800	0,4917	0,0309
2,4974	0,3474	0,1197	0,1816	0,0756	2,9004	3,0148	0,4828	0,0300
2,5820	0,3177	0,1115	0,1747	0,0734	3,0759	3,0491	0,4743	0,0291
2,6695	0,2909	0,1039	0,1681	0,0713	3,2607	3,0832	0,4664	0,0283
2,7600	0,2666	0,0969	0,1618	0,0692	3,4552	3,1171	0,4590	0,0275
2,8535	0,2446	0,0904	0,1557	0,0672	3,6599	3,1510	0,4520	0,0267
2,9501	0,2248	0,0844	0,1499	0,0653	3,8751	3,1847	0,4454	0,0259
3,0501	0,2068	0,0789	0,1443	0,0634	4,1012	3,2185	0,4392	0,0252
3,1534	0,1905	0,0737	0,1390	0,0616	4,3385	3,2523	0,4334	0,0244
3,2602	0,1757	0,0690	0,1338	0,0598	4,5875	3,2861	0,4280	0,0237

ERASMUS+ “GSEBS” : Arrigoni et al. “Blast waves and propagation and their mitigation”

3,3707	0,1622	0,0646	0,1289	0,0580	4,8486	3,3200	0,4229	0,0230
3,4849	0,1500	0,0605	0,1242	0,0563	5,1221	3,3541	0,4181	0,0224
3,6029	0,1389	0,0567	0,1196	0,0547	5,4085	3,3883	0,4137	0,0217
3,7250	0,1288	0,0532	0,1153	0,0531	5,7081	3,4226	0,4095	0,0211
3,8512	0,1196	0,0500	0,1111	0,0515	6,0214	3,4570	0,4056	0,0204
3,9817	0,1112	0,0469	0,1070	0,0500	6,3488	3,4915	0,4020	0,0198
4,1166	0,1035	0,0441	0,1031	0,0485	6,6906	3,5262	0,3985	0,0192
4,2560	0,0965	0,0415	0,0994	0,0471	7,0474	3,5610	0,3954	0,0187
4,4002	0,0901	0,0391	0,0958	0,0457	7,4194	3,5959	0,3924	0,0181
4,5493	0,0842	0,0369	0,0924	0,0443	7,8071	3,6309	0,3896	0,0176
4,7034	0,0788	0,0348	0,0891	0,0430	8,2109	3,6660	0,3870	0,0170
4,8628	0,0738	0,0328	0,0859	0,0417	8,6312	3,7011	0,3845	0,0165
5,0275	0,0693	0,0310	0,0828	0,0404	9,0685	3,7364	0,3823	0,0160
5,1978	0,0651	0,0293	0,0799	0,0392	9,5232	3,7717	0,3801	0,0155
5,3739	0,0613	0,0277	0,0770	0,0380	9,9957	3,8070	0,3781	0,0151
5,5560	0,0577	0,0263	0,0743	0,0368	10,4865	3,8424	0,3762	0,0146
5,7442	0,0544	0,0249	0,0717	0,0357	10,9960	3,8779	0,3744	0,0142
5,9388	0,0514	0,0236	0,0691	0,0346	11,5247	3,9133	0,3728	0,0137
6,1400	0,0485	0,0224	0,0667	0,0336	12,0730	3,9488	0,3712	0,0133
6,3480	0,0459	0,0212	0,0644	0,0325	12,6415	3,9844	0,3697	0,0129
6,5631	0,0435	0,0202	0,0621	0,0315	13,2307	4,0200	0,3683	0,0125
6,7854	0,0412	0,0192	0,0599	0,0305	13,8411	4,0556	0,3670	0,0121
7,0153	0,0391	0,0183	0,0578	0,0296	14,4732	4,0912	0,3658	0,0117
7,2530	0,0371	0,0174	0,0558	0,0287	15,1278	4,1270	0,3646	0,0114
7,4987	0,0353	0,0166	0,0539	0,0278	15,8053	4,1627	0,3634	0,0110
7,7528	0,0336	0,0158	0,0520	0,0269	16,5063	4,1986	0,3624	0,0107
8,0154	0,0319	0,0150	0,0502	0,0261	17,2318	4,2345	0,3613	0,0104
8,2870	0,0304	0,0143	0,0484	0,0253	17,9822	4,2705	0,3604	0,0100
8,5677	0,0290	0,0137	0,0468	0,0245	18,7584	4,3067	0,3595	0,0097
8,8580	0,0276	0,0131	0,0451	0,0237	19,5613	4,3430	0,3586	0,0094
9,1581	0,0264	0,0125	0,0436	0,0230	20,3916	4,3794	0,3578	0,0091
9,4683	0,0252	0,0119	0,0421	0,0223	21,2503	4,4160	0,3570	0,0088
9,7891	0,0240	0,0114	0,0406	0,0216	22,1383	4,4528	0,3562	0,0086
10,1207	0,0229	0,0109	0,0392	0,0209	23,0568	4,4898	0,3555	0,0083
10,4636	0,0219	0,0104	0,0379	0,0202	24,0069	4,5269	0,3548	0,0080
10,8181	0,0209	0,0100	0,0366	0,0196	24,9895	4,5644	0,3542	0,0078
11,1846	0,0200	0,0096	0,0353	0,0190	26,0061	4,6020	0,3536	0,0075
11,5635	0,0191	0,0092	0,0341	0,0184	27,0581	4,6399	0,3530	0,0073
11,9553	0,0183	0,0088	0,0329	0,0178	28,1467	4,6781	0,3525	0,0071
12,3603	0,0175	0,0084	0,0318	0,0172	29,2736	4,7166	0,3519	0,0068
12,7790	0,0167	0,0080	0,0307	0,0167	30,4402	4,7553	0,3515	0,0066
13,2120	0,0160	0,0077	0,0296	0,0162	31,6483	4,7943	0,3510	0,0064
13,6596	0,0153	0,0074	0,0286	0,0156	32,8995	4,8336	0,3506	0,0062

ERASMUS+ “GSEBS” : Arrigoni et al. “Blast waves and propagation and their mitigation”

14,1223	0,0146	0,0071	0,0276	0,0151	34,1958	4,8731	0,3502	0,0060
14,6008	0,0139	0,0068	0,0267	0,0147	35,5393	4,9129	0,3498	0,0058
15,0954	0,0133	0,0065	0,0258	0,0142	36,9319	4,9530	0,3494	0,0056
15,6068	0,0127	0,0062	0,0249	0,0137	38,3756	4,9933	0,3491	0,0054
16,1356	0,0122	0,0059	0,0240	0,0133	39,8727	5,0338	0,3488	0,0053
16,6822	0,0116	0,0057	0,0232	0,0129	41,4258	5,0745	0,3484	0,0051
17,2474	0,0111	0,0054	0,0224	0,0124	43,0371	5,1154	0,3481	0,0049
17,8317	0,0106	0,0052	0,0216	0,0120	44,7089	5,1564	0,3478	0,0048
18,4358	0,0101	0,0050	0,0209	0,0117	46,4440	5,1976	0,3475	0,0046
19,0604	0,0097	0,0047	0,0202	0,0113	48,2451	5,2388	0,3472	0,0045
19,7062	0,0092	0,0045	0,0195	0,0109	50,1145	5,2800	0,3470	0,0043
20,3738	0,0088	0,0043	0,0188	0,0106	52,0552	5,3213	0,3467	0,0042
21,0640	0,0084	0,0041	0,0182	0,0102	54,0697	5,3625	0,3464	0,0041
21,7776	0,0080	0,0040	0,0175	0,0099	56,1607	5,4036	0,3461	0,0039
22,5154	0,0076	0,0038	0,0169	0,0096	58,3308	5,4447	0,3458	0,0038
23,2782	0,0073	0,0036	0,0163	0,0092	60,5827	5,4856	0,3455	0,0037
24,0668	0,0070	0,0035	0,0158	0,0089	62,9185	5,5264	0,3452	0,0035
24,8822	0,0066	0,0033	0,0152	0,0086	65,3407	5,5670	0,3449	0,0034
25,7251	0,0063	0,0031	0,0147	0,0084	67,8512	5,6074	0,3447	0,0033
26,5966	0,0061	0,0030	0,0142	0,0081	70,4518	5,6477	0,3444	0,0032
27,4977	0,0058	0,0029	0,0137	0,0078	73,1440	5,6878	0,3442	0,0031
28,4293	0,0055	0,0027	0,0132	0,0076	75,9287	5,7279	0,3439	0,0030
29,3924	0,0053	0,0026	0,0128	0,0073	78,8065	5,7679	0,3437	0,0029
30,3882	0,0050	0,0025	0,0123	0,0071	81,7771	5,8079	0,3436	0,0028
31,4177	0,0048	0,0024	0,0119	0,0068	84,8400	5,8481	0,3434	0,0027
32,4821	0,0046	0,0023	0,0115	0,0066	87,9931	5,8886	0,3433	0,0026
33,5825	0,0044	0,0022	0,0111	0,0064	91,2343	5,9295	0,3433	0,0025
34,7202	0,0042	0,0021	0,0107	0,0062	94,5596	5,9712	0,3432	0,0024
35,8965	0,0040	0,0020	0,0103	0,0060	97,9643	6,0137	0,3432	0,0024
37,1126	0,0038	0,0019	0,0099	0,0058	101,4421	6,0575	0,3432	0,0023
38,3699	0,0037	0,0018	0,0096	0,0055	104,9852	6,1029	0,3432	0,0022
39,6698	0,0035	0,0017	0,0092	0,0054	108,5838	6,1503	0,3431	0,0021